PIEZOELECTRIC NANOGENERATOR BASED ON LEAD-FREE DOUBLE PEROVSKITE-PVDF FOR ENERGY HARVESTING APPLICATIONS

A thesis submitted towards partial fulfillment of requirements for

the degree of

Master of Technology in Nano science and Technology

Submitted by

SHUBHASIS MANDAL

ROLL NO.: M4NST22006

Registration No: 154575 of 2020-2021

Under the guidance of

Prof. (Dr). Kalyan Kumar Chattopadhyay

HOD of Department of Physics

Jadavpur University

Kolkata -700032

School of Materials Science and Nanotechnology

Course affiliated to

Faculty of Engineering and Technology

Jadavpur university

2022
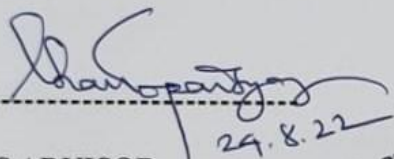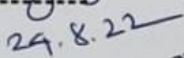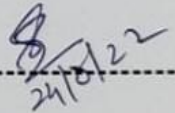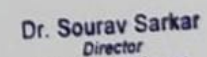
M.Tech. (Nanoscience and Technology)
course affiliated to
Faculty of Engineering and Technology
Jadavpur University
Kolkata, India

CERTIFICATE OF RECOMMENDATION

This is to certify that the thesis entitled "**Piezoelectric nanogenerator based on lead-free double perovskite-PVDF for energy harvesting applications**" is a reliable work carried out by **SHUBHASIS MANDAL** under our supervision and guidance for partial fulfilment of the requirement of Master of Technology in Nanoscience and Technology in School of Materials Science and Nanotechnology during the academic session **2020-2022**.

THESIS ADVISOR,

24.8.22

Dr. K. K. Chattopadhyay
Professor
Head, Department of Physics
Jadavpur University
Kolkata-700 032

Prof (Dr.) Kalyan Kumar
Chattopadhyay,
HOD of Department of Physics
Jadavpur University, Kolkata-700032.

DIRECTOR,

8/x/22
24/0

Prof (Dr.) Sourav Sarkar,
School of Materials Science
and Nanotechnology
Jadavpur University, Kolkata-700032

Dr. Sourav Sarkar
Director
Associate Professor
School of Materials Science & Nanotechnology
Jadavpur University
Kolkata - 700032

24 /08/2022

DEAN,
Prof. Subenoy Chakraborty,
Faculty Council of Interdisciplinary
Studies, Law and Management
Jadavpur University, Kolkata-700032.

Dean
Faculty of Interdisciplinary Studies
Law & Management
Jadavpur University, Kolkata-700032

DECLARATION OF ORIGINALITY AND COMPLIANCE OF ACADEMIC ETHICS

I hereby declare that this thesis contains literature survey and original research work by the undersigned candidate, as part of his **Master of Technology (Nano science and Technology)** studies during academic session **2020-2022**.

All information in this document has been obtained and presented in accordance with academic rules and ethical conduct.

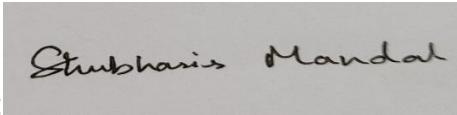I also declare that, as required by this rules and conduct, I have fully cited and referred all material and results that are not original to this work.

NAME: SHUBHASIS MANDAL

ROLL NUMBER: M4NST22006

THESIS TITLE: **Piezoelectric nanogenerator based on lead-free double perovskite-PVDF for energy harvesting applications**.

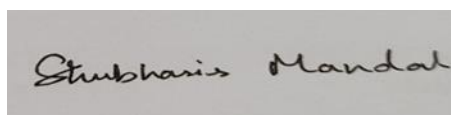SIGNATURE: *Shubhasis Mandal*   DATE:24.08.2022

Acknowledgement

I express my sincere gratitude to my supervisors **Prof. (Dr). Kalyan Kumar Chattopadhyay** under whose supervision and guidance this work has been carried out.It would have been impossible to carry out this thesis work with confidence without their wholehearted involvement, advice, support, and constant encouragement throughout. They have not only helped me in my thesis work but also have given valuable advice to proceed further in my life.

I also express my sincere gratitude to **Prof Dr. C.K. Ghosh, Prof Dr. Mahua Ghosh Chowdhury, Prof Dr. Sourav Sarkar**, Professor of School of Materials Science and Nanotechnology, Jadavpur University for their valuable suggestions.

I would also express my sincere thanks to **Mr. Suvankar Mondal**, Senior Research Scholar, and **Mr. Suvankar Poddar**, Junior Research Scholar of Department of Physics, Jadavpur University for their unconditional support and affection during my work.

I would also really like to thank all the staff members of School of Materials Science and Nanotechnology and Department of Physics for carrying out the critical characterization parts of the synthesized samples that composed a very important part of the thesis.

I am also grateful to my parents who have been my strength and inspiration throughout my M.Tech. course.

Date: August, 2022
Place: Jadavpur University

SHUBHASIS MANDAL (Exam Roll No: M4NST22006)

Abstract

As conventional energy sources deplete, a sustainable power source to satisfy the needs of energy requirements is critical in modern civilization. Bioenergy, hydropower, solar, and wind are some of the well-established renewable energy sources that assist meet the need for energy on a megawatt to gigawatt scale. In the rising era of IoT, nanogenerators based on nano energy are a developing technology that enables self-powered systems, sensors, and flexible and portable electronics (Internet of Things). Nanogenerators may capture small-scale energy from the environment and surroundings for effective use. The nanogenerators were based on piezoelectric, triboelectric, and pyroelectric effects, with Wang et al. developing the first of its kind in 2006. Because nanogenerators are lightweight, easily produced, sustainable, and maintenance-free devices, they represent a breakthrough in the field of ambient energy collecting techniques. The principles, performance, current breakthroughs, and use of nanogenerators in self-powered sensors, wind energy harvesting, blue energy harvesting, and their integration with solar photovoltaics are reviewed in detail in this study. Finally, the prognosis and problems for the advancement of this technology are discussed. This review focuses on the emergence and development of the promising benchmark lead-free double perovskite Cs2AgBiBr6. First, the structure-property relation, synthesis, and stability of Cs2AgBiBr6 are emphasized. Next, the fundamental optical and electronic properties, i.e., the absorption, photoluminescence, electron-phonon coupling, defects, charge carrier dynamics, and bandgap engineering, are discussed. Then, the recent progress in optoelectronic applications including solar cells, photo/X-ray detectors, and ferroelectric/magnetic devices, etc., are reviewed. Finally, the main challenges facing Cs2AgBiBr6 materials and related applications are presented alongside perspectives and possible solutions that may allow for the achievement of commercial, high-efficiency, stable, and nontoxic lead-free optoelectronic devices.

<u>CONTENTS</u>

Chapter 1

General Introduction

1.1. Nanostructures and nanotechnology

"biological system can be exceedingly small. Many of the cells are very tiny, but they are very active; they manufacture various substances; they walk around; they wiggle; and they do all kinds of marvellous things – all on a very small scale. Also, they store information. Consider the possibility that we too can make a thing very small which does what we want – that we can manufacture an object that maneuvers at that level."(From the talk **There's Plenty of Room at the Bottom**, delivered by Richard P. Feynman at the annual meeting of the American Physical Society [7].

The concept of nanotechnology was first mentioned by the famous physicist Richard Feynman in 1959 in his lecture which was published in 1960 entitled 'There's Plenty of Room at the Bottom' [7]. The word 'nano-technology' was first used by Norio Taniguchi in 1974 although it is not very well known. In 1986 inspired by Feynman's concept, K. Eric Drexler used the term 'nanotechnology' in book 'Engines of Creation: The Coming Era of Nanotechnology'[8].

Nanoscience is the science of objects with typical sizes of 1-100 nm. If matter is divided into such small objects the mechanical, electric, optical, and magnetic properties can change [9].Interfaces rather than bulk properties dominate. Quantum effects due to the size limitation come into play. Nanoscience and Nanotechnology are interdisciplinary, crossing boundaries between physics, chemistry, chemical, electric and mechanical engineering.

Nanoscience is one of the most important developments in the last decades. New technologies were required to enter the nanoscale because many of the traditional techniques do not work at the nanoscale. The relation between nanoscience and technology is like a symbiosis. Scientific discoveries lead to new technologies. The technology enables new fundamental insights. Two new technologies which enabled the progress of nanoscience are scanning tunnelling and

scanning force microscopy. They allow to image and manipulate objects on surfaces with sufficient precision even in ambient conditions or in liquids.

Nanotechnology literally means any technology on a nanoscale that has applications in the real world. Nanotechnology encompasses the production and application of physical, chemical, and biological systems at scales ranging from individual atoms or molecules to submicron dimensions, as well as the integration of the resulting nanostructures into larger systems. Nano technology is likely to have a profound impact on our economy and society in the early 21st century, comparable to that of semiconductor technology, information technology, or cellular and molecular biology. Science and technology research in nanotechnology promises breakthroughs in areas such as materials and manufacturing, nanoelectronics, medicine and healthcare, energy, biotechnology, information technology, and national security. It is widely felt that nanotechnology will be the next Industrial Revolution.

In the past few decades nanoscience and nanotechnology has been developed explosively due to discovery of novel synthesis routes, characterization techniques and manipulation tools. There are various types of nanoscale structures like, thin films, nanowires, nanoparticles etc. Nanoparticles are often called as quantum dots and can be considered as quasi zero-dimensional systems. It is nothing but basic physics acting behind the novel properties of the above-mentioned systems and it has been well explained by theoretical research. To understand these systems, it is very essential to discuss the density of states (DOS) of quantum dots (0 dimension), quantum wires (1 dimension) and quantum wells (2 dimensions) in brief.

The available electron states in a system can be calculated by the well-known Schrodinger's equation: $H\psi = E\psi$. Solving this we can finally get the density of states in k-space / volume as following,

$$\frac{dN(E)}{dE} = \frac{dN(k)}{dk} \times \frac{dk}{dE} = \begin{cases} \dfrac{1}{\pi\hbar}\sqrt{\dfrac{2m^*}{E}} & d=1 \\[4mm] \dfrac{m^*}{\pi\hbar^2} & d=2 \\[4mm] \dfrac{m^*\sqrt{2m^*E}}{\pi^2\hbar^2} & d=3 \end{cases}$$

In generalized form,

$$N(E)dE \propto E^{d/2-1}dE \qquad\qquad d=1,2,3$$

Here, d is the dimensionality, and the energy is measured from the top of the valence band for holes and from the bottom of the conduction band for electrons. In the 3D system, N(E) is a smooth square-root function of energy. In case of 2D system, N(E) is constant, therefore drastically changed from 3-D case. In 2-D system the energy spectrum is quasi-continuous, but the density of states is step function [10]. Every time when we go to a lower dimensionality system, the dependency of DOS on energy changes by E -1/2.
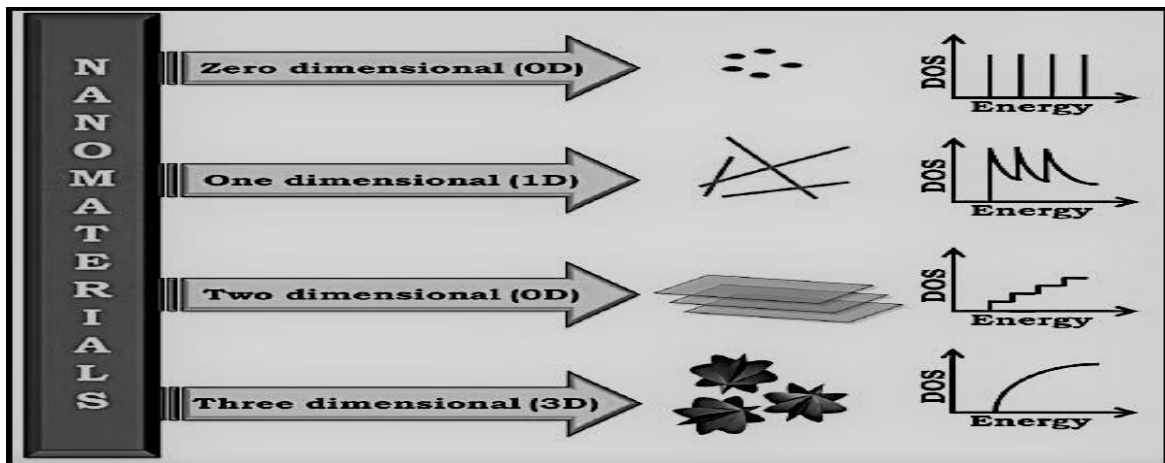
Fig 1.1 Schematic illustration of structural dimensionality of materials with density of states.

Now the "quantum size effect" should be briefly discussed. For this effect the electronic properties of materials are changed with pronounced reduction of its particle sizes. This effect does not play any role if the reduction of dimension is confined from macro to micro. Conversely, in the nanoscale, quantum effect becomes very prominent. When the sizes of the nanoparticles are equivalent to that of Bohr excitonic radius (rB) of those materials quantum confinement effect modifies the electronic structure of nanocrystals. If particle radius (r) in the nanocrystalline materials are less than Bohr radius (r <rB), strong quantum confinement effects take place. Weak quantum confinement effects are found within particles having radius larger than Bohr radius (r >rB).

A number of physical properties like electrical, optical, mechanical etc. change in nanoscale dimension compared to macroscopic system. For example, the increase in surface to volume ratio changes the thermal, mechanical and catalytic properties of materials. Reaction and diffusion rate for nanostructured materials and charge transport properties in nanodevices also become faster.

1.2. NANOGENERATOR

Nanogenerator technology is one of the most promising ways to harvest energy by converting mechanical/thermal energy as produced by small-scale physical change into electricity. Nanogenerator has three typical approaches: piezoelectric, triboelectric, and pyroelectric nanogenerators. Both the piezoelectric and triboelectric nanogenerators can convert the mechanical energy into electricity. However, the pyroelectric nanogenertors can be used to havest thermal energy from a time-dependent temperature fluctuation.

Nanowires

Piezoelectric nanowires (NWs) are the building blocks of NGs. NW is a one-dimensional (1D) nanomaterial that typically has a diameter less than 100 nm and a length more than 1 mm. Most ceramic NWs are single crystals. Compared to the conventional thin- film-based piezoelectric

cantilever transducers, using piezoelectric NWs for mechanical energy scavenging offers three unique advantages:

(1)   Enhanced piezoelectric effect. 400–500% enhancement of the piezoelectric effect was predicted due to the flexoelectric effect [18], when a strain gradient is experienced by a ferroelectric NW with a thickness of a few tens of nanometres.

(2)   Superior mechanical properties. The lattice perfection of NWs enables much larger critical strain, higher flexibility, and longer operational lifetime.

(3)   High sensitivity to small forces. Large aspect ratio and small thickness allow the creation of significant strain in the NWs under a force at the nano-Newton or even pico-Newton level.

1.3 PIEZOELECTRIC NANOGENERATORS

Energy can be stored in a capacitor, super capacitor, or battery. Capacitors are used when the application needs to provide huge energy spikes. Batteries leak less energy and are therefore used when the device needs to provide a steady flow of energy.

Current interest in low power energy harvesting is for independent sensor networks. In these applications an energy harvesting scheme puts power stored into a capacitor then boosted/regulated to a second storage capacitor or battery for the use in the microprocessor. The power is usually used in a sensor application and the data stored or is transmitted possibly through a wireless method.

Nanotechnology is one of the most promising innovations capable of effective energy harvesting. Nanogenerator is a technology that converts mechanical/thermal energy as produced by small-scale physical change into electricity. . Both the piezoelectric and triboelectric nanogenerators can convert the mechanical energy into electricity. However, the pyroelectric nanogenerators can be used to harvest thermal energy from a time-dependent temperature fluctuation.

Piezoelectric Nanogenerator is an energy harvesting device converting the external kinetic energy into an electrical energy based on the energy conversion by nano-structured piezoelectric material. Although its definition may include any types of energy harvesting devices with nano-structure converting the various types of the ambient energy (e.g., solar power and thermal energy), it is used in most of times to specifically indicate the kinetic energy harvesting devices utilizing nano-scaled piezoelectric material.

Although still in the early stage of the development, it has been regarded as a potential breakthrough toward the further miniaturization of the conventional energy harvester, possibly leading the facile integration with the other types of energy harvester converting the different types of energy and the independent operation of mobile electronic devices with the reduced concerns for the energy source, consequently.

1.4. MECHANISM OF PIEZOELECTRIC NANOGENERATORS
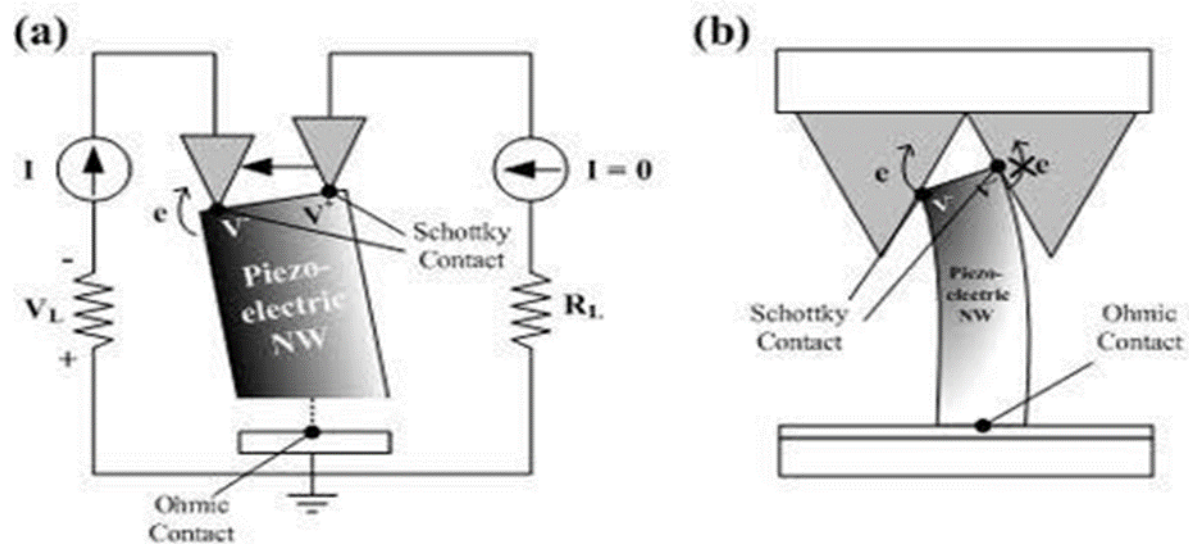
Fig. 1

Fig 1 Working principle of nanogenerator where an individual nanowire is subjected to the force exerted perpendicular to the growing direction of nanowire. (a) An AFT tip is swept through the tip of the nanowire. Only negatively charged portion will allow the current to

flow through the interface. (b) The nanowire is integrated with the counter electrode with AFT tip-like grating. As of (a), the electrons are transported from the compressed portion of nanowire to the counter electrode because of Schottky contact.
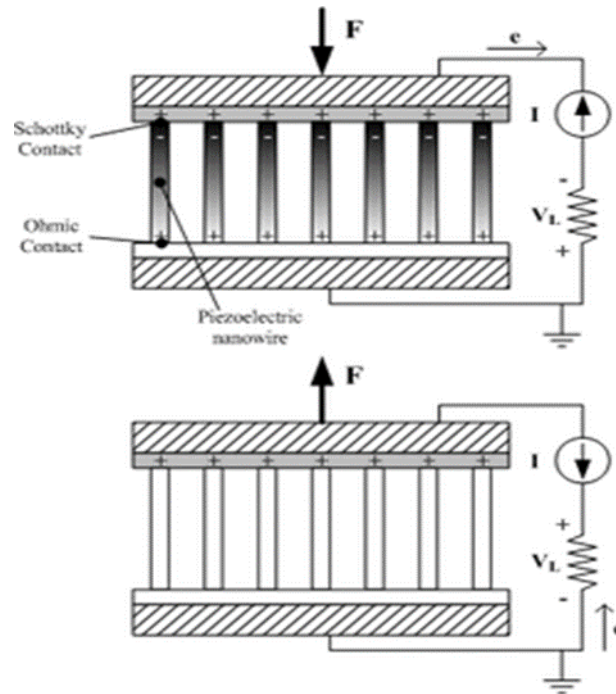
Fig. 2

Fig.2 Working principle of nanogenerator where an individual nanowire is subjected to theforce exerted parallel to the growing direction of nanowire.

The working principle of nanogenerator will be explained for 2 different cases: the force exerted perpendicular and parallel to the axis of the nanowire.

The working principle for the first case is explained by a vertically grown nanowire subjected to the laterally moving tip (fig.1). When a piezoelectric structure is subjected to the external force by the moving tip, the deformation occurs throughout the structure. The piezoelectric effect will create the electrical field inside the nanostructure; the stretched part with the positive strain will exhibit the positive electrical potential, whereas the compressed part with the negative strain will show the negative electrical potential. This is due to the relative displacement of cations with respect to anions in its crystalline structure. As a result, the tip of

the nanowire will have an electrical potential distribution on its surface, while the bottom of the nanowire is neutralized since it is grounded. The maximum voltage generated in the nanowire can be calculated by the following equation:

$$V_{max} = \pm \frac{3}{4(\kappa_0 + \kappa)}[e_{33} - 2(1+\nu)e_{15} - 2\nu e_{31}]\frac{a^3}{l^3}\nu_{max}$$

where κ_0 is the permittivity in vacuum, κ is the dielectric constant, e_{33}, e_{15} and e_{31} are the piezoelectric coefficients, ν is the Poisson ratio, a is the radius of the nanowire, l is the length of the nanowire and ν_{max} is the maximum deflection of the nanowire's tip.

The electrical contact plays an important role to pump out charges in the surface of the tip. The schottky contact must be formed between the counter electrode and the tip of the nanowire since the ohmic contact will neutralize the electrical field generated at the tip. In order to form an effective schottky contact, the electron affinity (Ea) must be smaller than the work function(φ) of the metal composing the counter electrode.

For the second case (Fig.2), a model with a vertically grown nanowire stacked between the ohmic contact at its bottom and the schottky contact at its top is considered. When the force is applied toward the tip of the nanowire, the uniaxial compressive is generated in the nanowire. Due to the piezoelectric effect, the tip of the nanowire will have a negative piezoelectric potential, increasing the Fermi level at the tip. Since the electrons will then flow from the tip to the bottom through the external circuit as a result, the positive electrical potential will be generated at the tip. The schottky contact will barricade the electrons being transported through the interface, therefore maintaining the potential at the tip. As the force is removed, the piezoelectric effect diminishes, and the electrons will be flowing back to the top in order to

neutralize the positive potential at the tip. The second case will generate alternating current output signal.

1.5. SOURCES FOR ENERGY HARVESTING

The classification of energy harvesting can be organized on the basis of the form of energy they use to scavenge the power. The various sources for energy harvesting are wind turbines, photovoltaic cells, thermoelectric generators and mechanical vibration devices such as piezoelectric devices, electromagnetic devices etc.

2.1   Mechanical Vibrations

When a device is subjected to vibration, an inertial mass can be used to create movement. This movement can be converted to electrical energy using three mechanisms: piezoelectric, electrostatic and electromagnetic. The form of energy utilized here is the mechanical energy.

2.1.1   Piezoelectric Energy Harvesting

The piezoelectric effect was discovered by J and P Curie in 1880. They found that if certain crystals were subjected to mechanical strain, they became electrically polarized and the degree of polarization was proportional to the applied strain. Conversely, these materials deform when exposed to an electric field. These materials can convert mechanical energy from pressure, vibrations or force into electricity. This property of piezoelectric materials is considered by the researchers to develop various piezoelectric harvesters in order to power different applications. Due to their inherent ability to detect vibrations, piezoelectric materials have become a viable energy scavenging source. Widely used materials are materials such as quartz (naturally occurring), Polycrystalline ceramic , Lead Zirconium Titanate . With their anisotropic characteristics, the properties of the piezoelectric material differ depending upon the direction of forces and orientation of the polarization and electrodes. The properties of piezoelectric materials vary with age, stress and temperature. The possible advantages of using piezoelectric materials are the direct generation of desired voltage since they do not need a separate voltage

source and additional components. These generators are compatible with the MEMs. These generators are the simplest and can be used in force and impact- coupled harvesting applications. Some disadvantages are that piezoelectric materials are brittle in nature and sometimes allow the leakage of charge.
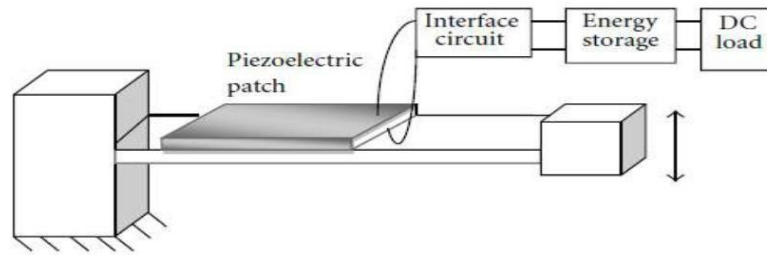
Fig 2.1 piezoelectric energy harvesting system
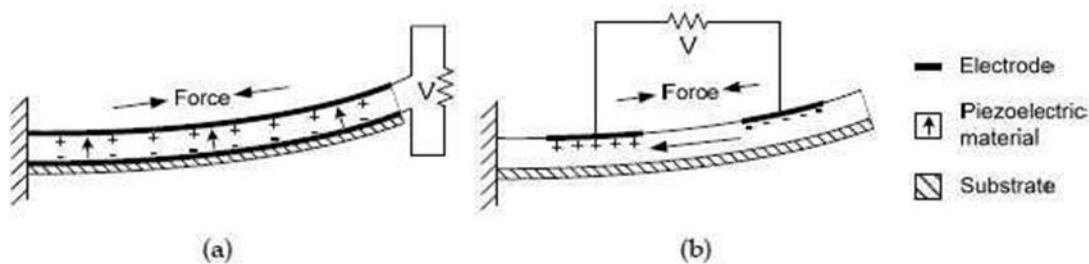
Fig 2.2 Two types of piezoelectric energy harvesters (a) d31 mode (b) d33 mode

Piezoelectric energy harvesters can work in either d33 mode or d31 mode as shown in Fig. 2.2. In d31 mode, a lateral force is applied in the direction perpendicular to the polarization direction. Here the electrodes are on its top and bottom surfaces of the bending beam as in Fig. 2.2(a). In d33 mode, force applied is in the same direction as the polarization direction but has all electrodes on its top surfaces as in Fig. 2.2(b). Although piezoelectric materials in d31 mode normally have a lower coupling coefficient than in d33 mode, d31 mode is more commonly used. This is because when a cantilever or a double-clamped beam (two typical structures in

vibration energy harvesters) bends, more lateral stress is produced than vertical stress, which makes it easier to couple in d31 mode.

1.5.1 Nano generators Based on Piezoelectric Effect:

Piezoelectric nanogenerators (PENG) work on the principle of piezoelectric effect, which means electricity generation when subjected to mechanical stress. In PENG, two electrodes with balanced fermi levels on a piezoelectric material are subjected to an external strain, which creates a piezo potential difference between the internal and external Fermi levels (highest energy state occupied by the electrons) at the contacts. To balance this difference in Fermi levels, the charge carriers flow through the external load and a balanced electrostatic level is reached. Alternatively, applying an electric field on a piezoelectric material can cause a mechanical strain. There are two cases of PENG, one where the individual nanostructure (nanowire/nanorod) is subjected to the strain exerted perpendicular to the growing direction of the nanowire/nanorod, which leads to the generation of the electric field.In PENG, two electrodes with balanced fermi levels on a piezoelectric material are subjected to an external strain, which creates a piezo potential difference between the internal and external Fermi levels (highest energy state occupied by the electrons) at the contacts. To balance this difference in Fermi levels, the charge carriers flow through the external load and a balanced electrostatic level is reached. Alternatively, applying an electric field on a piezoelectric material can cause a mechanical strain. There are two cases of PENG, one where the individualnanostructure (nanowire/nanorod) is subjected to the strain exerted perpendicular to the growing direction of the nanowire/nanorod, which leads to the generation ofthe electric field. When the force is applied perpendicular to its axis. When a forceis applied perpendicular to the direction of the axis of the nanostructure using atomic force microscopy probe, one portion of the nanostructure is stretched(positive strain) while the other undergoes compression (negative strain). The stretched surface with positive potential was first contacted by the probe, and at this interface,

the bias voltage is negative. Thus, a reversed bias Schottky diode is formed with little current. When the probe contacts the compressed side of the nanostructure with negative potential, a biased positive voltage is formed at the interface with sharp peak output current as driven by the potential difference between the two sides. The current flow due to the ohmic contact formed at the bottom of the nanostructure finally re-balances the electric field generated at the tip. The conduction is possible only when the top electrode is in contact with the negative potential, whereas no current will be generated if the top electrode is in contact with the positive potential. This is the case for n-type semiconductive nanostructures; in the case of p-type semiconductive nanostructures, it will exhibit the reverse phenomenon since the hole is mobile in this case. The other case is where the external strain is exerted parallel to the growing direction of the nanostructures. When the force is applied to the tip of the laterally grown nanowire which is stacked between the Schottky contact and ohmic contact, a uniaxial compressive is generated in the nanowire. The tip of the nanowire will have negative potential and increases the Fermi level due to the piezoelectric effect. As the electrons flow from the tip of the nanowire to the bottom through the external circuit, positive potential will be generated at the tip. The Schottky contact blocks the flow of electrons through the nanowires and instead passes the electrons through the external circuit. When the applied force is removed, the piezoelectric effect diminishes immediately and a positive potential at the tip gets neutralized because of the migration of electrons from the bottom electrode to the top, which produces voltage peak in the opposite direction. Due to the in-situ rectifying effect of the Schottky contact, the detected output exhibits direct current characteristics.

In their work, Zhu et al. replaced this Schottky contact with PMMA layer to create a potential barrier for charge accumulation. In this nanogenerator, when compressive force is applied, a piezopotential field is generated along the nanowires. As a result of electrostatic force, inductive charges accumulate on the top and bottom of the electrodes. This is similar to

capacitive configuration in which the strained nanowires can be compared with polarized dipole moments in aplate capacitor filled by a dielectric material. Once the applied stress is released, the piezopotential disappears and the electrons flow through the external circuit. AC output is observed in the cases of capacitive configuration and when the Schottky diode is a series resistance in the piezoelectric nanogenerators.

To effectively enhance the output power of PENG, several nano wires are stacked together to effectively synchronize the voltage output of each nanowire. Two effective integrations of nanowires were developed by Wang. one is vertical- nanowire-integrated nanogenerator in which the vertically grown nanowires are stacked together. The working mechanism of vertically integrated PENGs includes lateral bending and vertical compression of nanowires as explained earlier. The other one is the lateral-nanowire-integrated nanogenerator, in which the parallelly grown nanowires are stacked together in the nanogenerator. Inlaterally integrated nanogenerators, the deformation of nanowires is always causedby lateral bending either by bending the substrate or by applying pressure on the radial direction of the nanowires. The uniform lateral bending of nanowires can beregarded as the lateral stretching by neglecting the strain distribution in the radial direction due to the ultra-high aspect ratio of the 1D nanostructures. In a study, theenergy conversion efficiency of both laterally stretched nanowire and vertically compressed nanowire were compared, and the results showed that the laterallybent nanowire could generate higher voltage than the compressed one.
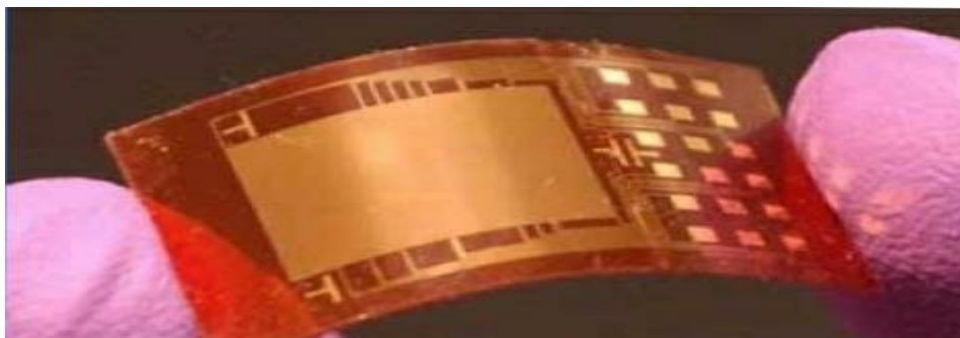
Figure 3: Piezoelectric Material

1.6. Applications of PENG:

A. PENGs acts as a sustainable power supply for various smart applications like self-powered nano/microsensors, self-powered electronics, wearable/flexible electronics, and biomedical applications.

B. Chemically reinforced composite-based PENG produces a maximum AC voltage of 65 V, which is converted into DC output using a filling wave bridge rectifier to charge capacitors and power LEDs.

C. PENGs were also used in solar PV cells for improved power conversion efficiency. A tandem nanogenerator was developed by integrating silicon nanopillar solar cell with PVDF nanogenerator; this device was capable of harvesting energy from both sound waves and solar energy. It is a silicon-based nanoheterostructure photovoltaic device, which is based on the piezo-phototronic effect. The efficiency of the solar cell was improved from 8.97% to 9.51%.

D. An organic piezoelectric nanogenerator based on multilayer structure of PVDF NFL mats, followed by PEDOT coating, which exhibits an open circuit voltage of 48 Volts under the stress of 8.3 kPa. This power output suggests its application in the field of self-powered wearable and portable electronics.

E. This makes it capable of noise detection, wind energy harvesting, security monitoring, and also useful in self-powered sensors. There are several security systems sensors like transport monitoring, wireless sensors, and biomedical sensors based on PENGs, which holds practical importance.

1.7. What are perovskites:

Perovskite materials, named after the 19th century Russian mineralogist Lev Perovskite, feature a crystal-lattice structure of inorganic molecules similar to ceramics, as well as organic molecules interwoven throughout.

Perovskites are a crystal family with potential features for applications in nanotechnology, particularly nanostructured solar cells. The name 'perovskite' refers to a class of materials that have a characteristic crystal structure of cuboid and diamond forms. They have long piqued the curiosity of scientists due to their superconducting, electronic, and ferroelectric capabilities.

Since it was revealed that perovskite solar cells are also extraordinarily effective at capturing photons of light and converting them into an electric current, research interest in them has soared.

Crystals are orderly arrangements of atoms, molecules, or ions that repeat themselves in all directions. We encounter crystals all the time in everyday life - ordinary salt, diamond, snowflakes. What is maybe less well-known is that when crystals are lowered to the nanoscale, they exhibit highly intriguing features. There, we enter the world of nanocrystals, structures that have shown to be incredibly valuable in the construction of technological applications on extremely small sizes.

Quantum dots are man-made semiconducting nanoparticles with only a few thousand atoms. Researchers have researched how electrons interact with light in perovskite quantum dots to learn more about the underlying physics of these materials.

Crystals are organized arrangements of atoms, molecules, or ions that repeat in all directions. In regular life, we come across crystals all the time: common salt, diamonds, and snowflakes. What is maybe less well-known is that certain crystals exhibit highly intriguing features when their size is decreased to the nanoscale. There, we enter the world of nanocrystals, structures

that have shown to be particularly valuable in the construction of technological applications on microscopic sizes.

Quantum dots are man-made nanoparticles of semiconducting material with only a few thousand atoms. Researchers investigated the underlying physics of perovskite quantum dots by studying how electrons interact with light in these materials.

1.7.2 Perovskite structures:

Despite the basic perovskite crystal structure's simplicity, this class of compounds exhibits a wide range of structural alterations and variations.

Perovskite ('real perovskite') is a mineral comprised of calcium, titanium, and oxygen in the form $CaTiO_3$. A perovskite structure, on the other hand, is anything with the generic form ABX_3, variable composition, and the same crystalline structure as perovskite (the mineral).

A, B, and X can indicate a mixture of organic and inorganic ions. A is an organic cation, B is a large inorganic cation, and X_3 is a tiny halogen anion (often oxide) that links to both cations.

Perovskites can have a wide range of fascinating features depending on which atoms/molecules are employed in the structure, including superconductivity, enormous magnetoresistance, spin-dependent transport (spintronics), and catalytic capabilities. As a result, perovskites provide an interesting playground for physicists, chemists, and material scientists.

Perovskites are found in nature mostly as oxides, the majority of which are silicates (such as bridgmanite crystals), but they also occur as fluorides, chlorides, hydroxides, arsenides, and intermetallic complexes. While natural perovskite minerals are few in number, synthetic perovskites span the entire periodic table in terms of elemental composition and can exist in a variety of complex formulas such as metallic perovskites, hybrid organic-inorganic perovskites, metal-free perovskites, and even noble gas-based perovskites.

The bulk of efficient perovskites are tunable bandgap semiconductor lead metal halides.
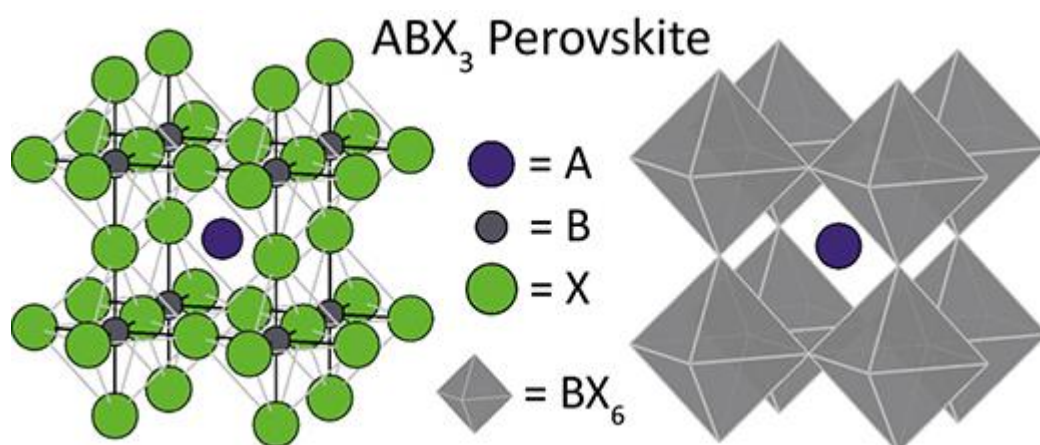
Standard depiction of the aristotype cubic perovskite. Shown in display styles evidencing either all the atoms (left) or only the BX6 octahedral network and A atoms (right). (Source: doi:10.1021/acsenergylett.0c00039)

1.7.3. Perovskite applications:

Lasers made of perovskite

Perovskite cells excel not only at absorbing light, but also in emitting it, according to researchers.

Recently, researchers used single perovskite alloy nanowires to create a globally and continuously programmable nano laser.

X-ray detector made of perovskite

Researchers used 3D aerosol jet printing to 3D print perovskite layers on a graphene substrate. The end product was beautiful. The technology yielded X-ray detectors with unprecedented sensitivity, representing a fourfold increase over best-in-class medical imaging systems.

These highly efficient perovskite X-ray detectors that can be easily integrated into standard microelectronics to considerably improve the performance of medical imaging devices.
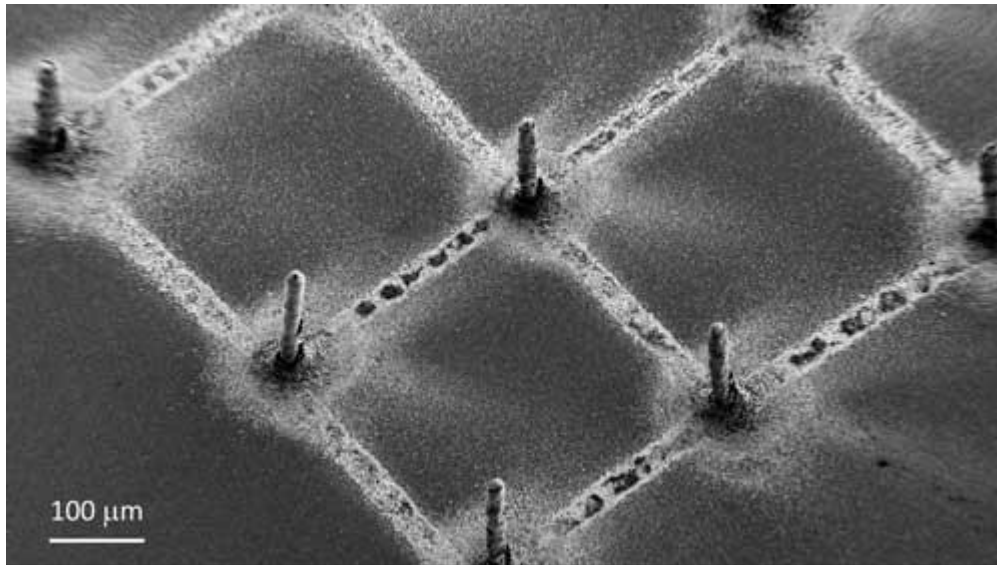
Example of the deposited perovskite pillars, defining a pixel for the creation of an image. (Image: L. Forró, EPFL)

Perovskite nanoantenna's that emit light

Based on halide perovskite, researchers created innovative effective nanoscale light sources. Perovskite nanoparticles act as both emitters and nanoantennas, allowing for enhanced light emission without the use of additional devices.

Furthermore, by altering the composition of the material, perovskite allows for the adjustment of emission spectra across a visible range. As a result, the novel nanoparticles offer a viable foundation for the development of tiny optoelectronic devices such as optical chips, light-emitting diodes, and sensors.

3D-printed perovskite nano pixels

The three-dimensional (3D) geometry of 3D-printed nano pixels can increase the emission brightness of display pixels, varying with the height of the pixels, and can be used to fabricate super high-resolution devices. Researchers demonstrated 3D printing of perovskite nanopillars that can be used for creating nanoscale display pixels.

2.1. Introduction: The Emergence of Lead-Free Perovskites

Lead (Pb) halide perovskites, with a general chemical formula of ABX3, where A is a CH3NH3 + (MA+), CH(NH2)2 + (FA+) or Cs+ cation, B is a Pb2+ cation and X is Cl–, Br– or I– anion, have attracted tremendous attention in both scientific and industrial fields in the last 10 years. Lead-based perovskites have demonstrated exceptional optoelectronic properties such as a suitable and tuneable direct bandgap, strong light absorption, long carrier lifetime and diffusion length, small and balanced carrier effective mass, easy solution fabrication, high structural diversity, and high defect tolerance. Such remarkable properties make perovskite a versatile material for a wide range of applications such as solar cells, photodetectors, light-emitting devices, photocatalysis, X-ray imaging, lasing and luminescent solar concentrators Among these applications, lead-based perovskite solar cells (PeSCs) are best known, having achieved a state-of-the-art power conversion efficiency (PCE) of 25.5% for a single-junction laboratory-scale device and a 29.5% record PCE for a perovskite/silicon tandem monolithic device. This progress has been achieved through fabricating high-quality perovskite films and optimizing device interface contact to minimize energy losses. Additionally, lead-based perovskite light-emitting diodes (PeLEDs) now have also delivered high external quantum efficiencies (EQEs) over 20% through suppression of non-radiative recombination and improvement of light out-coupling efficiency. Despite the notable progress in perovskite optoelectronic devices, lead perovskites still suffer from two major issues, i.e., the lack of stability and Pb toxicity. Indeed, lead halide perovskite films are sensitive to ambient conditions (oxygen and water), prolonged illumination, and high temperatures, leading to fast material degradation. Although considerable efforts have been devoted to improving the stability of PeSCs, their lifetime is still far behind the warranty of 25 years for commercial PV modules. Furthermore, for PeLEDs, its operational stability is even worse than PeSCs, with most reported lifetimes (T50) generally limited to tens to hundreds of hours, due mainly to ion migration, electrochemical reactions,

and interfacial reactions. The toxicity of Pb presents another big obstacle for future commercialization. Pb is a particularly insidious bioaccumulative hazard that has the potential to cause irreversible health problems. While perovskite devices are carefully encapsulated and lead ions are rationally captured by lead-absorbing materials and strictly recycled, the prevention of Pb leakage into the environment cannot be guaranteed. To tackle these issues, significant efforts have been committed to developing lead-free perovskites, in the hope to combine the impressive optoelectronic properties of lead-based perovskites with high stability and nontoxicity. As the superior properties of lead perovskites originate from the unique electronic configuration of Pb $6s^2$, divalent tin (Sn^{2+}) and germanium (Ge^{2+}) in the same group with similar lone pair were first used to replace Pb. However, Sn and Ge-based perovskites show very poor stability because of the rapid oxidation of Sn^{2+} and Ge^{2+} to +4 states. Furthermore, Sn might be even more toxic than Pb for human beings upon dispersion into the environment. An emerging and promising method is to use one monovalent and one trivalent metal cation to replace the position of Pb in the crystal structure, forming so-called ordered double perovskites with a general chemical formula of $A_2B^+B^{3+}X_6$. This strategy is very effective because it maintains the 3D perovskite structure and at the same time offers more material diversity. Through combining different A, B^+, B^{3+} and X elements (for example, A = K, Rb, Cs; B^+ = Li, Na, K, Rb, Cs, Ag; B^{3+} = Al, Ga, In, Sb, Bi, Sc, Y, and X = F, Cl, Br, I), more than 100 double perovskites with a structural tolerance factor and octahedra factor in a reasonable range have been predicted to be thermodynamically stable. Therefore, the structural and functional diversity, combined with the high stability observed in double perovskites, make them very promising lead-free candidates for a wide range of optoelectronic applications.

2.2. Lead-Free Double Perovskite Cs2AgBiBr6: Structure

2.2.1 Structure and Chemical Bonds

Typical double perovskites implement a heterovalent substitution strategy of using a monovalent and a trivalent metal cation to replace Pb and retain the 3D connectivity of the structure. The crystal structure evolution from standard PVDF to Cs2AgBiBr6 and its derivatives as well as representative band structures are presented in Figure 1. Lead perovskite PVDF (Figure 4a) utilizes a cubic structure (space group Pm3m) at high temperature over 327 K, with the octahedra maintained by IPbI bond angle of 90° and PbI bond length of 3.136 Å. As shown in the inset of Figure 1a the valence band maximum (VBM) of PVDF consists mainly of the antibonding states of Pb s and I p orbitals, and conduction band minimum (CBM) is composed of the antibonding states of Pb p and I s orbitals, which results in the direct bandgap with high absorption. Note that the I orbital is omitted in the schematic. Cs2AgBiBr6 displays a similar cubic double perovskite structure with a space group of Fm3m (lattice parameter 11.27 Å) at room temperature (RT). This so-called rock salt ordering structure is formed by alternating corner-connected $[AgBr_6]^{5-}$ and $[BiBr_6]^{3-}$ octahedra in all three directions with Cs+ located at the framework cavities (Figure 1b). The configuration of the octahedra, including the volume variation and distortion/tilting (mainly associated with bond lengths and bond angles), have a significant effect on the electronic structure and thus determine the optoelectronic properties of the perovskites. In ordered Cs2AgBiBr6, the corresponding Ag-Br/Bi-Br and Ag-Br-Bi bonds all maintain a 90° or 180° angle, and the bond length for Ag-Br and Bi-Br is comparable (2.804–2.828 Å). A shorter bond length compared with PVDF means the electrons are more tightly bound to the atoms, contributing to stronger bond strength and stiffness in the Cs2AgBiBr6 framework. Basically, the $[AgBr_6]^{5-}$ and $[BiBr_6]^{3-}$ octahedra volume are determined by the metal ionic radius (1.15 and 1.03 Å for Ag+ and Bi3+, respectively), the electronegativity (1.93 and 2.02 for Ag+ and Bi3+,

respectively) and the interaction from neighboring octahedra, which yield a combined result of complex volume variation such as expansion or contraction of octahedra. The tilting/distortion of octahedra is partially caused by the mismatch of the octahedral sublattice, and to accommodate this mismatch, strain relaxation will modify the bond lengths/ angles. Experimentally, detailed structural information can be obtained from the Raman vibrational modes and refinement of X-ray diffraction (XRD) patterns. The corresponding band structure of Cs2AgBiBr6 is simplified in inset of Figure (4b) revealing that the VBM is composed of Ag d, Bi s character and CBM has Ag s, Bi p character which locate at different positions. Here the Br p orbital that contributes to both VBM and CBM is omitted as well in the schematic. Hence the hybridization between Ag and Bi orbitals at band edges is responsible for the indirect bandgap nature. Although Cs+ orbitals do not make obvious contributions near band edges, they can have an impact on the band structure through bonding interaction between Cs+ and the metal framework. Understanding the structure-property relationship is important to design and achieve Cs2AgBiBr6 based materials with desirable optoelectronic properties. For example, a homogenous octahedral contraction and shrinkage of Bi−Br− Ag bonds in Cs2AgBiBr6 can promote the overlap of elemental orbitals and thus lead to bandgap narrowing. Under thermal treatment, Cs2AgBiBr6 will show a lattice expansion with varied Ag-Br and Bi-Br bond length and the thermal expansion coefficient of Ag-Br bond is obviously larger than the Bi-Br bond, suggesting that variation of the Ag-Br bond is the main contributor to lattice thermal expansion. These anharmonic fluctuations of Ag-Br and Bi-Br bonds change the energy band structure, which are one of the main factors for the observed thermochromism of Cs2AgBiBr6 crystals and films.
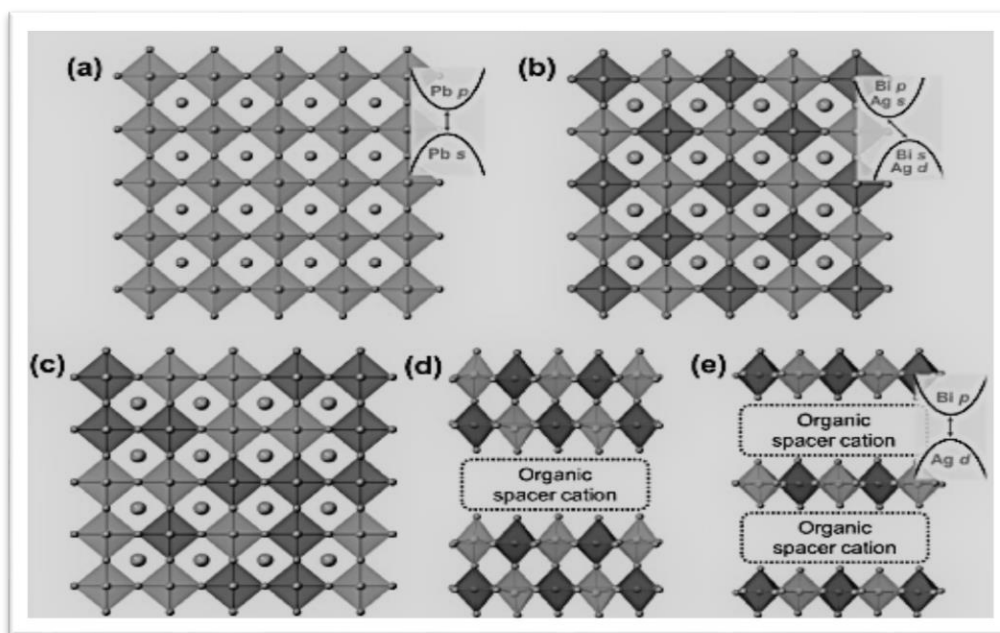
Figure 4. Structure evolution and band structures of perovskites. a) lead-based PVDF, b) ordered Cs2AgBiBr6, c) disordered Cs2AgBiBr6, d) RP Cs2AgBiBr6 derivatives, n = 2, e) DJ Cs2AgBiBr6 derivatives, n = 1. Insets of a), b) and e) present the corresponding band structures with the arrow representing the lowest-energy transition.

2.2.2 Atomic Arrangement

Apart from chemical bond variation, the atomic arrangement in Cs2AgBiBr6 can also significantly affect the band structure and optoelectronic properties. Here the metal atomic arrangement is discussed, i.e., the cation order/disorder of Ag and Bi octahedra (Figure 4b, c). Similarly, B+/B3+ alternate cation order also heavily influences the optoelectronic properties especially the magnetic and ferroelectric properties of oxide double perovskites A2B+/B3+O6. In a regularly ordered crystal structure, each [AgBr6] 5– octahedra is surrounded by six [BiBr6] 3– octahedra and vice versa. It should be noted that the solution processing of Cs2AgBiBr6 films or crystals will cause vacancies, interstitials, and antisites including Ag-on-Bi and Bi-on-Ag, leading to lattice disorder. Experimentally, the disordered behavior can be observed in the XRD pattern because of the different scattering effects of Ag+ and Bi3+ and the reduced symmetry in the disordered structure. The degree of the disorder can be simply determined by comparing the peak intensity of the super lattice order-related plane (111) and the normal lattice-related reflection plane (022), with a higher ratio representing a higher order extent. The

atomic arrangement in the double perovskite has a big effect on its optoelectronic properties, including bandgaps, lattice distortion, defects, and carrier mobility. By manipulating cations from ordered to disordered, Cs2AgBiBr6 shows enhanced light absorption in the visible and near-infrared region, with the band structure changing from 1.46 eV indirect to 0.44 eV pseudo direct bandgap, providing a promising method to improve light absorption of Cs2AgBiBr6. The bandgap narrowing arises from the altering of band hybridization in the reduced crystal symmetry caused by disordered arrangement of [AgBr6] 5– and [BiBr6] 3– octahedra. Unfortunately, this strategy requires very high temperatures (beyond 1200 K) which greatly limit practical applications. Strategy of using additives such as phenylethylamine bromide (PEABr) can effectively increase the ordering degree because of the selective coordination effect between the functionalized groups in PEA+ and metal framework. Ordered crystals present less lattice distortion, reduced defect density, suppressed trapped-exciton formation, enhanced carrier mobility, hence superior X-ray detection performance. For potential optoelectronic applications, disordered antisites are attributed to deep-level defects, which decrease the carrier mobility and cause carrier recombination in Cs2AgBiBr6.Therefore, to obtain highly ordered Cs2AgBiBr6, researchers need to pay attention to the key growth factors such as using moderate temperature, slower synthesis speed, higher pressure, suitable additives or dopants in the material fabrication process.

2.1.3. Layered Structure:

To modulate the properties of Cs2AgBiBr6 double perovskite such as a transition from indirect to direct bandgap, or selectively tune the bandgap, layered Cs2AgBiBr6 derivatives have been developed based on specific organic spacer cations, forming homologous compounds with stoichiometries of R4AgBiX8, R2CsAgBiX7, and R2AgBiX8 which adopt the single layer (n = 1) Ruddlesden-Popper (RP) structure, bilayer (n = 2) RP structure (Figure 4d) and single-layer Dion-Jacobson (DJ) structure (Figure 4e), respectively. However, layered Cs2AgBiBr6

derivatives with a DJ structure (n = 2) or n values greater than 2 for RP and DJ structure have not been demonstrated experimentally so far. A wide choice of organic cations is available because layered structures do not have a strict restriction on the length or size of the interlayer organic spacer cations. Representative bulky R cations in $Cs_2AgBiBr_6$ derivatives are monovalent alkyl-ammonium cations such as propylammonium (PA, $CH_3(CH_2)_2NH_3^+$), butylammonium (BA, $CH_3(CH_2)_3NH_3^+$), and divalent cations such as 1,4-butanediammonium (BDA, $(CH_2)_4(NH_3)_2^+$). [30,31] To choose a specific R cation for a potential optoelectronic application, one should consider the interaction between the inorganic framework and the organic cations. Generally, R cations that have smaller interlayer distance and stronger hydrogen bonding, coupled with π–π interactions, would generate higher charge transport efficiency in the layered perovskite. R cations can also be selectively tailored to be highly luminescent or to contribute to perovskite ferroelectricity. The incorporation of R cations causes obvious distortion or tilting of the perovskite lattice (related to the Ag-halide-Bi bond and metal-halide bond), crystalizing the lattice in a monoclinic or triclinic system with lower symmetry. Compared with the $[BiBr_6]^{3-}$ octahedra, the distortion of $[AgBr_6]^{5-}$ octahedra is more pronounced, with a larger deviation in the equatorial and axial Ag-Br bond lengths, arising from the mixing of filled Ag- nd orbitals with empty (n+1) s orbitals.

Regarding the properties of low-dimension $Cs_2AgBiBr_6$ derivatives, their optical bandgaps are usually larger than their 3D counterparts, with minimal difference between varied R cations, therefore further understanding is needed to explain what contribution the R cation makes to the structure and properties of $Cs_2AgBiBr_6$. The indirect bandgap of $Cs_2AgBiBr_6$ becomes direct in most cases when the inorganic framework becomes a monolayer, with the typical band structure shown in the inset of Figure 1e. This direct transition originates from the single-metal-orbital contributions to the VBM and CBM of layered $Cs_2AgBiBr_6$ derivatives in the case of n = 1. This dimension reduction would result in more pronounced lattice

distortion and reshaping the orbital composition of the band edges. Given that the corresponding photoluminescence is usually too weak to be observed at RT and the more distorted structure, layered Cs2AgBiBr6 perovskite derivatives presently appear to have limited optoelectronic applications. However, these low dimensional perovskites offer a research platform for self-trapping emission arising from electron-phonon coupling, or ferroelectric, ferro/antiferromagnetic, and spin-electronic applications.

2.3. Other Applications

Cs2AgBiBr6 has also provided new opportunities in energy related photocatalysis. The basic photocatalytic mechanism involves the absorption of photons to generate electrons and holes, charge separation and migration to the reaction sites, and chemical oxidation/reduction reactions mediated by the photoinduced electrons and holes. Besides the traditional standards for photocatalytic materials (high light absorption, efficient charge separation, and appropriate redox ability), Cs2AgBiBr6 has enhanced operational chemical stability under different catalytic conditions like strong acidic/basic solutions and highly reducing/oxidizing atmospheres. Typically, Cs2AgBiBr6 nanocrystals could convert CO_2 into solar fuels such as CO and CH4, affording an impressive total electron consumption of 105 µmol g−1 over 6 h, with no H2 side product detected. Beyond CO_2 reduction, the successful application of Cs2AgBiBr6 has also been demonstrated in dye degradation and H2 generation. Because of its high humidity-dependence of the electrical properties, Cs2AgBiBr6 thin film can also work as a humidity sensor, showing fast response time (1.78 s) and recovery time (0.45 s).

References:

[1] Newton, Marshall D., et al. "Electron transfer in chemistry." (2001).

[2]   ArnulfJager-Waldau, Solar Energy Materials and Solar Cells, Volume 95, Issue 6, June2011, Pages 1509–1517

[3]   K. Aryal, B. N. Pantha, J. Li, J. Y. Lin, and H. X. Jiang, Applied Physics Letters 96,052110 (2010)

[4] Ludmila P. Oleksenko, Nelly P. Maksymovych, Evgeniy V. Sokovykh, Igor P. Matushko,

      Andrii I. Buvailo, Norman Dollahon, Sensors and Actuators B 196 (2014) 298–305

[5] A. Ohtomo, M. Kawasaki, T. Koida, K. Masubuchi, H. Koinuma, Y. Sakurai, Y. Yoshida,

   T. Yasuda, and Y.Segawa, Applied Physics Letters 72, 2466 (1998)

[6]   Ryu Abe, Kazuhiro Sayama, and Hideki Sugihara, J. Phys. Chem. B 2005, 109, 16052-16061

[7]   R. P. Feynman, A lecture in engineering science, In California Institute of Technology,Feb. edn. 1960.

[8] Drexler, K. Eric. Engines of creation.Anchor, 1986.

[9] R. G. Gordon, MRS Bull. 25 (2000) 52

[10] P. Motiarty, Rep. Prog. Phys. 64 (2001) 297.

[11] Kuo-Feng Lin, Hsin-Ming Cheng, Hsu-Cheng Hsu, Li-Jiaun Lin, Wen-Feng Hsieh, Chemical Physics Letters 409 (2005) 208–211

[12]   O. Vigil, F. Cruz, A. Morales-Acevedob, G. Contreras-Puente, Materials Chemistry andPhysics 68 (2001) 249–252 [13] G. Anil Kumar, M. V. Ramana Reddy, KattaNarasimha Reddy, Journal of Physics: Conference Series 365 (2012) 012031

[14]   H. Merzouk, A. Chelouche, S. Saoudi, D. Djouadi, A. Aksas, ApplPhys A (2012)109:841–84

[15].   BP Energy Economics. BP Energy Outlook, 2018 ed.; BP p.l.c.: London, UK, 2018.

[16].   Hu, Y.; Wang, Z.L. Recent progress in piezoelectric nanogenerators as a sustainable power source in

self-powered systems and active sensors. Nano Energy 2014, 14, 3–14. [CrossRef]

[17].   Beeby, S.P.; Tudor, M.J.; White, N.M. Energy harvesting vibration sources for microsystems applications.

Meas. Sci. Technol 2006, 17, 175–195. [CrossRef]

18.   Batra, A.K.; Alomari, A. Ambient Energy Sources: Mechanical, Light, and Thermal. In Power Harvesting via

Smart Materials; SPIE Press: Bellingham, WA, USA, 2017; pp. 1–15. ISBN 9781510608498.

[19].   Wang, Z.L. Self-Powered Nanotech. Sci. Am. 2008, 298, 82–87. [CrossRef] [PubMed]

[20].   Schiffer, M.B. Draw the Lightning Down: Benjamin Franklin and Electrical Technology in the Age of Enlightenment;

University of California Press: Berkeley, CA, USA, 2006; Volume 408.

[21].   Kagan, C.R.; Fernandez, L.E.; Gogotsi, Y.; Hammond, P.T.; Hersam, M.C.; Nel, A.E.; Penner, R.M.; Willson, C.G.;

Weiss, P.S. Nano Day: Celebrating the Next Decade of Nanoscience and Nanotechnology. ACS Nano 2016, 10,

9093–9103. [CrossRef]

[22].   Wang, Z.L. Piezoelectric Nanogenerators Based on Zinc Oxide Nanowire Arrays. Science 2006, 312, 242–246.

[CrossRef] [PubMed]

[23].   Kumar, B.; Kim, S.W. Energy harvesting based on semiconducting piezoelectric ZnO nanostructures.Nano Energy 2012, 1, 342–355. [CrossRef]

[24].   Askari, H.; Khajepour, A.; Khamesee, M.B.; Saadatnia, Z.; Wang, Z.L.
Piezoelectric and triboelectric

nanogenerators: Trends and impacts. Nano Today 2018, 22, 10–13

[25].   Action Nechibvute, Albert Chawanda, Pearson Luhanga; Department of Physics, Midlands State University, Gweru, Zimbabwe & Department of Physics, University of Botswana, Gaborone, Botswana ―Piezoelectric Energy Harvesting Devices: An Alternate Energy Source for Wireless Sensors‖.

[26].   Minbaek Lee, Joonho Bae, Joohyung Lee, Churl-Seung Lee, Seunghun Hongb and Zhong Lin Wang ―Self-powered environmental sensor system driven by nanogenerators‖.(pages 3359-3363)

[27].   Sravanthi Chalasini & James M Conrad, Electrical and Computer Engineering, University of North Carolina at Charlotte ―A Survey of Energy Harvesting Sources for Embedded Systems‖.

[28].   Xudong Wang, Department of Materials Science and Engineering, University of Wisconsin–Madison, WI 53706, USA ―Piezoelectric nanogenerators—Harvesting ambient mechanical energy at the nanometer scale‖.

[29] M. A. Green, A. Ho-Baillie, H. J. Snaith, Nat. Photonics 2014, 8, 506.

[2] S. Bai, P. Da, C. Li, Z. Wang, Z. Yuan, F. Fu, M. Kawecki, X. Liu, N. Sakai, J. T.-W. Wang, S. Huettner, S. Buecheler, M. Fahlman, F. Gao, H. J. Snaith, Nature 2019, 571, 245.

[30] M. V. Kovalenko, L. Protesescu, M. I. Bodnarchuk, Science 2017, 358, 745.

[31] Y. Zhao, K. Zhu, Chem. Soc. Rev. 2016, 45, 655.

[32] NREL Best Research-Cell Efficiency Chart, https://www.nrel. gov/pv/assets/pdfs/best-research-cell-efficiencies.20200104.pdf

(accessed: April 2021).

[33] X.-K. Liu, W. Xu, S. Bai, Y. Jin, J. Wang, R. H. Friend, F. Gao, Nat. Mater. 2021, 20, 10.

[34] C. Kuang, Z. Hu, Z. Yuan, K. Wen, J. Qing, L. Kobera, S. Abbrent, J. Brus, C. Yin, H. Wang, W. Xu, J. Wang, S. Bai, F. Gao, Joule 2021, 5, 618.

[35] J. Li, H.-L. Cao, W.-B. Jiao, Q. Wang, M. Wei, I. Cantone, J. Lü, A. Abate, Nat. Commun. 2020, 11, 310.

[36] T. Zhang, Z. Cai, S. Chen, ACS Appl. Mater. Interfaces 2020, 12, 20680.

[37] W. Pan, H. Wu, J. Luo, Z. Deng, C. Ge, C. Chen, X. Jiang, W.-J. Yin, G. Niu, L. Zhu, L. Yin, Y. Zhou, Q. Xie, X. Ke, M. Sui, J. Tang, Nat. Photonics 2017, 11, 726.

[38] B. Wang, N. Li, L. Yang, C. Dall'Agnese, A. K. Jena, S.-i. Sasaki, T. Miyasaka, H. Tamiaki, X.-F. Wang, J. Am. Chem. Soc. 2021, 143, 2207.

[39] F. Brivio, J. M. Frost, J. M. Skelton, A. J. Jackson, O. J. Weber, M. T. Weller, A. R. Goñi, A. M. A. Leguy, P. R. F. Barnes, A. Walsh, Phys. Rev. B 2015, 92, 144308.

[40] S. Jiang, Y. Fang, R. Li, H. Xiao, J. Crowley, C. Wang, T. J. White, W. A. Goddard III, Z. Wang, T. Baikie, J. Fang, Angew. Chem., Int. Ed. 2016, 55, 6540.

Chapter -2

Literature Review

Literature review:

The manipulation of matter on an atomic, molecular, and supramolecular scale is known as nanotechnology ("nanotech"). The National Nanotechnology Initiative later adopted a more generalized definition of nanotechnology, defining it as the manipulation of matter with at least one dimension scaled from 1 to 100 nanometers. As a result, the plural term "nanotechnologies" as well as "nanoscale technologies" are frequently used to refer to the vast spectrum of research and applications that share the property of size.

Thin film technology may be used on a variety of substrate materials, including metals, ceramics, and polymers. Silicon, glass, and steel are all typical substrate materials. The qualities of the substrate material can be improved, enhanced, and customized to match the special needs of a certain application by carefully selecting the technique and deposition materials. Furthermore, thin film technologies that may be applied to flat substrates or objects with highly complicated geometrical forms are now accessible.

Thin film deposition materials can range from metals and pure elements to more complicated compounds such as oxides, nitrides, and polymers. Most source materials require high degrees of purity to enable effective thin film coating characteristics. Deposition materials with purity greater than 99.99% are not rare.

The SOL-GEL technology is an extremely successful thin film deposition process. The sol-gel process is a wet-chemical method that is used mostly in materials science and ceramic engineering. These techniques are generally used to create materials (usually metal oxides) from a colloidal solution (sol) that serves as a precursor for an integrated network (or gel) of discrete particles or network polymers. Metal alkoxides and metal salts (such as chlorides,

nitrates, and acetates) are common precursors that undergo different types of hydrolysis and polycondensation processes.

S.M Attia, Jue Wang, Guangmin WU, Jun Shen and Jianhua "Review **on sol-gel drived coatings: process, technique and optical applications"**, journal of materials science and technology, vol-18, no-3, 2002. here conventional sol-gel technique is briefly discussed.

But this technique is not automatic and requires manual control which is not appropriate for preparing uniform thin films.

Md. Feroz Ali, Utpal Saha and M.F.Hossain* "**Design an Automatic Dipping and Withdrawing System for the Deposition of Thin Films**" ICECTE2012. In this paper an automatic length-controlled sol- gel system is designed which can deposit thin film for 2cm, 3cm, 4cm, 5cm,6cm,7cm.

But this system requires the use of ribbon which is very much subjected to vibration and the dipping and withdrawing speed cannot be controlled in this system.

Shuva paul "**Optimization of microcontroller based automatic sol-gel method with respect to optical proparties of ZnO films**" B.Sc. Dissertation, EEE, RUET, 2013. in this paper a digital sol-gel system is proposed.

This system was designed to solve the problem of using ribbon by using mechanical gear but it was not completely vibration less.

Ayesa Tuz Johra Shilpy "**Fabrication of digital SOL-GEL coating system and characterization of prepared ZnO thin films with respect to optical properties**" B.Sc.

Dissertation, EEE, RUET, 2016. In this paper a digital sol-gel system was proposed and Rack and pinion was replaced by rod and friction wheel.

But the weight of the machine was too small to reduce the vibration of the motor and friction in the rod and pinion caused non uniform motion of the substrate holder.

Yashaswi Soniab, UpasanaRani, Akash Shukla,**" "Transition metal-based halides double Cs$_2$ZSbX$_6$ (Z = Ag, Cu, and X = Cl, Br, I) perovskites: A mechanically stable and highly absorptive materials for photovoltaic devices"**

The electronic transport properties have been calculated within the constant relaxation time approximation. Seebeck coefficient is noted to decreasing with increasing temperature and figure of merits are increasing with increasing temperature at a given electron and hole concentration (1018-1021 cm−3). The figure of merit signifies that these materials may also be used as thermoelectric devices. These computational observations hereby are of paramount importance for future integrated applications.

Lijun Lu 1 , Wenqing Ding 1 , Jingquan Liu, Bin Yang " **Flexible PVDF based piezoelectric nanogenerators**", journal of materials science and technology Piezoelectric PVDF and its copolymers have been widely concerned because of their good flexibility, strength, easy processing, low cost and other advantages. They have been widely used in sensors and actuators so far, indicating the broad application prospect. In this paper, we summarize the recent progress of flexible PVDF-based piezoelectric sensors and nanogenerators, mainly focuse on the materials selection and incorporation, fabrication process, structural design and energy harvester application.

Satyaranjan Bairagi , S. Wazed Ali* "**Flexible lead-free PVDF/SM-KNN electrospun nanocomposite based piezoelectric materials: Significant enhancement of energy harvesting efficiency of the nanogenerator**". In this paper an   Piezoelectric energy

harvesting is an emerging technology to harvest green energy from different sources in our surrounding . To demonstrate the essence of piezoelectric energy harvesting system, researchers have developed various piezoelectric materials like lead zirconate titanate (PZT), barium titanate (BaTiO3), poly (vinylidene difluoride) (PVDF) and so forth [2e4]. The composite based piezoelectric materials have also been explored very successfully to reduce the individual limitations of ceramic and poly-mer based piezoelectric materials.

Xiaole Cao, Yao Xiong, Jia Sun, Xiaoxiao Zhu,* Qijun Sun,* and Zhong Lin Wang* "**Piezoelectric Nanogenerators Derived Self-Powered Sensors for Multifunctional Applications and Artificial Intelligence**" B In this review, we introduce the rapid development of materials, fabrication, performance enhancement in the field of PENGs, and their applications in mechanical energy harvesting and self-powered multifunctional sensors. Ever since the invention of PENGs, its rapid development has inspired many research fields from energy harvesting to self-powered systems. On one hand, substantial efforts have been devoted to enhancing the output performance of PENGs, achieving several orders of magnitude enhancement

Sumera Rafique a,b,* , Ajab Khan Kasi a , Aminullah a,c , Jafar Khan Kasi a , Muzamil Bokhari a , Zafar Shakoor " **Fabrication of Br doped ZnO nanosheets piezoelectric nanogenerator for pressure and position sensing applications**" In this research, a unique strategy was developed to enhance the output performance of 2D ZnO nanosheets based piezoelectric nanogenerator (PENG). The Br doped 2D ZnO nanosheets were fabricated by facile hydrothermal method on nanoporous anodic aluminum oxide (AAO) template. Along with structural and optical characterization of Br doped 2D ZnO nanosheets, the electrical output performance of Br doped 2D ZnO PENG was demonstrated under external mechanical force.

Simadri Badatya, Dhiraj Kumar Bharti, Natarajan Sathish, Avanish Kumar Srivastava, and Manoj Kumar Gupta* Humidity "**Sustainable Hydrophobic Poly(vinylidene fluoride)-Carbon Nanotubes Foam Based Piezoelectric Nanogenerato**r" in this research, Light weight lead free, polymer, and carbon nanotubes based flexible piezoelectric nanogenerators have prompted widespread concern for harvesting mechanical energy and powering next generation electronics devices. Herein, lightweight polyvinylidene fluoride (PVDF)-carbon nanotube (CNT) foam was prepared to fabricate humid resistant hydrophobic flexible piezoelectric nanogenerator to converts mechanical energy into electricity for the first time.

Anh Thi Le, Mohsen Ahmadipour, Swee-Yong Pung* "**A review on ZnO-based piezoelectric nanogenerators: Synthesis, characterization techniques, performance enhancement and applications**" In this article, the development of ZnO-based PNGs from synthesis nanostructures to device design and recent applications was reviewed. With an interest in flexible devices, hydrothermal synthesis appears to be the most commonly used method to produces ZnO NRs arrays for PNGs application. A summary of several measurement techniques involved to investigate the piezoelectric property of ZnO NRs as well as to measure the output current and voltage of the fabricated device.

Pengcheng Jiao,"**Emerging artificial intelligence in piezoelectric and triboelectric nanogenerators**" This review article discusses the advent and development of piezoelectric nanogenerators (PENG) and triboelectric nanogenerators (TENG), and envision the future trend of deploying artificial intelligence (AI) in the nanogenerators to obtain AI-PENG and AI-TENG with desirable electrical performance. We explain why the energy harvesting technologies are considered as one of the dominant green energy solutions, what the technological challenges that PENG and TENG have been facing in the current stage, and how

to surpass the limits of PENG and TENG using AI. Following the review of the existing studies in the literature, we envision the potential research avenues and emerging trends for AI-PENG and AI-TENG for future innovations.

Tae-Hoon Kong, Sang-Seok Lee, Geon-Ju Choi, and Il-Kyu Park "**Churros-like Polyvinylidene Fluoride Nanofibers for Enhancing Output Performance of Triboelectric Nanogenerators**" In summary, the surface roughness and phase of the PVDF NFs were modulated by controlling the solvent evaporation kinetics by varying the RH without adding a foreign additive during the electrospinning. As the RH was increased from 10 to 70%, the specific surface area increased gradually and finally formed a churros-like structure. In addition, the β phase ratio in the PVDF NFs was affected by the RH and increased drastically over the RH range between 20 and 45%, which was attributed to the difference between the wet-bulb temperature and dew point of the mixed solvents. As the RH was increased from 10 to 70%, the output voltage and current increased dramatically from 14 to 234 V and from 0.5 to 11 μA, respectively. Therefore, the maximum output power increased from 5 to 1738 μW/cm2 , which was enough to turn on an array of 60 series-connected LEDs without using any charge storage circuits.

Yanhong Li, Zhihao Zhao, Lu Liu, Linglin Zhou, Di Liu, Shaoxin Li, Shengyang Chen, Yejing Dai,* Jie Wang,* and Zhong Lin Wang "**Improved Output Performance of Triboelectric Nanogenerator by Fast Accumulation Process of Surface Charges**" In summary, it has been demonstrated that using fast charge accumulation process on dielectric material with high relative permittivity is an effective approach to achieve high equilibrium state of surface charges and high output performance of TENG. Compared with the limited surface charges generated by triboelectrification of common TENG, fast charge accumulation can break

through the limitation of triboelectrification on surface charge density, which is also conducive to broaden the materials selection range of TENG. Therefore, benefit from the high relative permittivity of P(VDF-TrFE) together with fast charge accumulation, surface charge density reaches 2.20 mC m−2 , while the contact efficiency can be increased to 82%. In addition, it is expected to further raise the equilibrium state of surface charges through using dielectric materials with appropriate thickness, higher relative permittivity, and low leakage current. Besides, we also demonstrate that fast charge accumulation is greatly advantageous for boosting output performance under high humidity environment, which provides an instructive method for how to maintain the output performance of TENG working in high humidity environments.

Hongwei Lei,* David Hardy, and Feng Gao* "**Lead-Free Double Perovskite Cs2AgBiBr6: Fundamentals, Applications, and Perspectives**" The recent progress on the wide applications including solar cells, light/X-ray detectors, and ferroelectric/magnetic devices are highlighted. Moreover, the challenges of Cs2AgBiBr6 materials and related applications are discussed and perspectives are provided for guiding the future development of this research area.

Gnanasam panthan, Abiram Fatemeh, Heidari Gourji, Punniamoorthy Ravirajan ,Thanihaichelvan Murugathas, Dhayalan Velauthapillai, "**Air Processed Cs2AgBiBr6 Lead-free Double Perovskite High-mobility Thin Film Field-effect Transistors**" This review article discusses A FET with a lead free Cs2AgBiBr6 perovskite thin film channel was successfully demonstrated. The Cs2AgBiBr6 thin film fabricated by recrystallizing the pre-prepared Cs2AgBiBr6 solution followed by annealing at 285°C enhanced the grain growth and resulted with a maximum grain size of 412 (±44) nm. The channel length of the FET strongly

influenced the on current, threshold voltage and hole mobility of the FETs. All three parameters were reduced with increasing channel length. The strong dependency of on current and mobility on the channel length confirmed the dominance of grain boundaries in the electrostatic gating in Cs2AgBiBr6 thin film FETs. The lower mobility and on-current in the longer channel FET can be attributed to the increased charge scattering at the effectively larger number of grain boundaries of the longest Cs2AgBiBr6 thin film. The maximum mobility of 0.29 ($\pm$00.07) cm2V -1s -1 observed in the FETs with 30 μm channel was two orders of magnitude higher than the previously reported hole mobility of the same material due to the much larger grain size.

Kijoo Eom, Young-Eun Shin, Joong-Kwon Kim, Se Hun Joo, Kyungtae Kim, Sang Kyu Kwak, Hyunhyub Ko, Jungho Jin, and Seok Ju Kang "**Tailored poly(vinylidene fluoride-co-trifluoroethylene) Crystal Orientation for a Triboelectric Nanogenerator through Epitaxial Growth on a Chitin Nanofiber Film"** In this paper The crystallographic match between the chitin and PVDFTrFE enables the development of the intended crystal orientation, with the PVDF-TrFE polarization axis aligned perpendicular to the substrate. In addition, the epitaxially grown PVDF-TrFE on chitin not only enhances the performance of the TENG but also increases the stability of the hygroscopic chitin film against water. The corresponding TENG exhibits a significantly higher output current compared to that of a non-epitaxial PVDFTrFE/chitin film. Furthermore, the triboelectric sensors based on epitaxial PVDF-TrFE/chitin films allow the monitoring of subtle pressures, suggesting that tailoring the crystal orientation of PVDF-TrFE is a promising approach for developing high-performance TENGs.

Reference:

[1]   https://www.reference.com/science/summary-nanotechnology d44deb56a9de7125?qo=cdpArticles, Accessed on October 15,2016

[2]   Lu, G. Q. & Zhao, X. S. Nanoporous materials- an overview. Series on Chemical Engineering 4, 1-13 (2004).

[3]   Rao, C. N. R., Mueller, A. & Cheetham, A. K. Nanomaterials - An introduction. Chemistry of Nanomaterials 1, 1-11 (2004).

[4]   Kear, B. H. & Skandan, G. Overview: status and current developments in nanomaterials. International Journal of Powder Metallurgy (Princeton, New Jersey) 35, 35-37 (1999).

[5]   Tolles, W. M. & Rath, B. B. General overview on nanomaterials. Nanomaterials: Synthesis, Properties and Applications, 545-553 (1996).

[6]   Shūichi Kinoshita "Structural colors in the realm of nature" World Scientific Publishing 2008 pages 3–6

[7]   Donald M. Mattox "the foundations of vacuum coating technology" pp-43

[8]   Madhobilata, Mst. N. Tamanna, M. F. Hossain, M. Fardousi "design and fabrication of a simple cost effective spi coater for deposition of thin film." International conference on Electrical, Computer and telecommunication engineering, vol 1, ICECTE2012,RUET, rajshahi-6204, Bangladesh

[9]   http://www.renewableenergyworld.com/articles/2014/07/7-reasons-thin-film-is-alive-and-set-to-win-in-solar.html, Accessed on October 16, 2016

[10]   https://en.wikipedia.org/wiki/Nanotechnology, Accessed on October 15, 2016

[11]   http://www.bccresearch.com/blog/report-archives/importance-thin-film-industry.html , Accessed on October 16,2016

[12]   http://en.wikipedia.org/wiki/Sol-gel

[13]   Allhoff, Fritz, Patrick, Moore, Daniel "what is nanotechnology and why does it matter? from science to ethics. John Wiley and Sons. Pp. 3-5"

[14]   https://en.wikipedia.org/wiki/Applications_of_nanotechnology, Accessed on October 15, 2016

[15]   Karn, Barbara; Todd Kuiken; Martha Otto (2009-12-01). "Nanotechnology and in Situ Remediation: A Review of the Benefits and Potential Risks". Environmental Health Perspectives 117 (12): 1823–1831.

[16]   Qu, Xiaolei; Alvarez, Pedro J J; Li, Qilin (2013). "Applications of nanotechnology in water and wastewater treatment". Water research 47 (12): 3931–46.

[17]   https://depts.washington.edu/spirolab/researchpro.html. Accessed January 07, 2014

[18]   Ayesa Tuz Johra Shilpy "Fabrication of digital SOL-GEL coating system and characterization of prepared ZnO thin films with respect to optical properties" B.Sc. Dissertation, EEE, RUET, 2016.

[19]   Madhobilata, Mst. N. Tamanna, M. F. Hossain, M. Fardousi "design and fabrication of a simple cost effective spi coater for deposition of thin film." International conference on Electrical, Computer and telecommunication engineering, vol 1, ICECTE2012, RUET, rajshahi-6204, Bangladesh

[20]   Krisna sinha "a handbook of deposition process and techniques" pp.30-32

[21]   Bunshah, R. F., (ed), "Deposition Technologies for Films and Coatings:Developments

Chapter -3

Instrument and apparatus

Instrument and apparatus

In this chapter major apparatus and accessories which were used while synthesis, are discussed along with the working principle and the operation of different characterization techniques has been given.

3.1 Crystal Structure Analysis

3.1.1. X-RAY Diffractometer

In the year 1895, the German physicist Roentgen discovered X-rays and so named due to the unknown nature at that time. These rays were invisible, traveled in straight lines and affected the photographic plate like ordinary light. Also, these rays show more penetrating power than light. In the year 1912, the exact nature of X-rays and diffraction phenomenon of x-rays by atomic planes of crystals were properly discovered. This discovery showed the wave nature of X-rays and explored a new direction to investigate the structure of matter. Solid matter canbe divided as follows:

- **Amorphous:** The atoms are arranged in a random way similar to the disorder we findin a liquid. Glasses are amorphous materials.

- **Crystalline:** The atoms are arranged in a regular pattern, and one smallest volume element that by repetition in three dimensions describe the crystal. This smallest volume element is called a unit cell. The dimensions of the unit cell are described by three axes: a, b, c and the angles between them alpha (α), beta (β), gamma (γ). About 95% of all solids can be described as crystalline. X-rays are electromagnetic radiation of almost same nature as light but having shorter wavelength of 0.5 to 2.5 Å regions. X-rays occupy the region between gamma and ultraviolet rays in the entire spectrum.

X-rays are electromagnetic radiation of almost same nature as light but having shorter wavelength of 0.5 to 2.5 Å regions. X-rays occupy the region between gamma and ultraviolet rays in the entire spectrum.
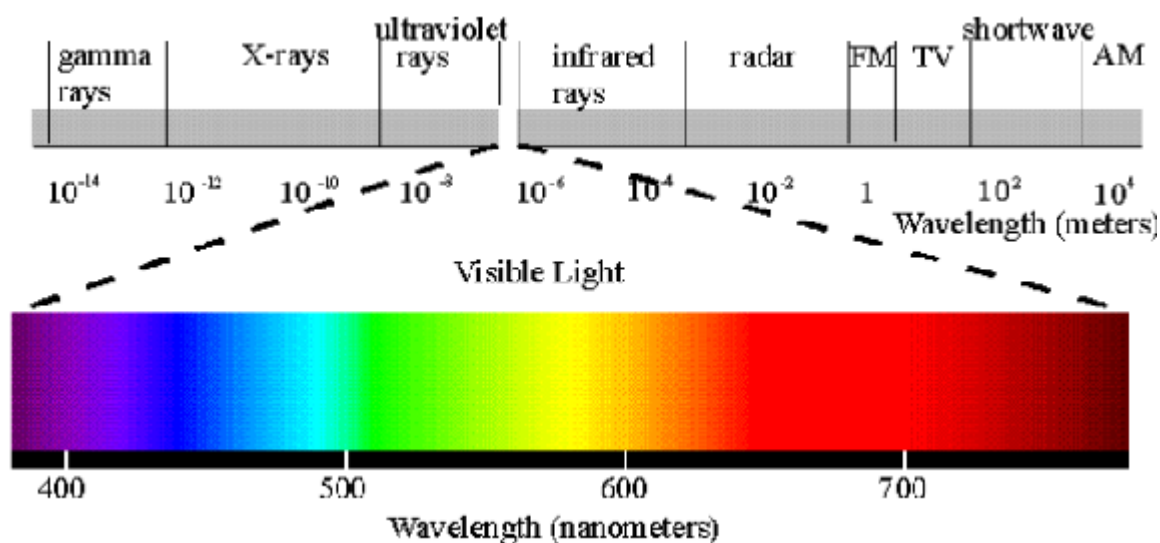
Fig 3.1: Illustration of electromagnetic spectrum

Diffraction is a scattering phenomenon in which a large number of atoms participate and act as scattering center. X-rays scattered by the atoms which are periodically arranged in the lattice, have definite phase relationship in between them. In some scattering direction, destructive interference takes place but, in few directions, constructive interference occurs andforms the diffracted beam. *"A diffracted beam may be defined as a beam composed of a large number of scattered rays mutually reinforcing one another."*

- **Working Principle**

In XRD, a collimeter beam of X-rays is incident on a specimen and is diffracted by the crystalline phases in the specimen. Using Bragg equation for first order diffraction, lattice spacing may be found from the diffraction angles. *Bragg's law* is the basic law which governs the X-ray diffraction technique of structural analysis. In *Bragg's law,* the interaction between x-rays and the electrons of the atoms is described as a process of reflection of x-rays by the atomic planes. When mono chromatic x-rays incident on the atoms in the crystal lattice, atomic planes allow a part of x-rays to pass through and reflect the other part, there exist a path difference in between the reflected rays from plane 1 and plane 2. These rays willreinforce each other, only when this path difference is equal to an integral multiple of the wavelength.

The *Bragg's law* can be written as: **2dsinθ = nλ**

Where **n** is an integer and **λ** is the wavelength of the x-rays used, **θ** is

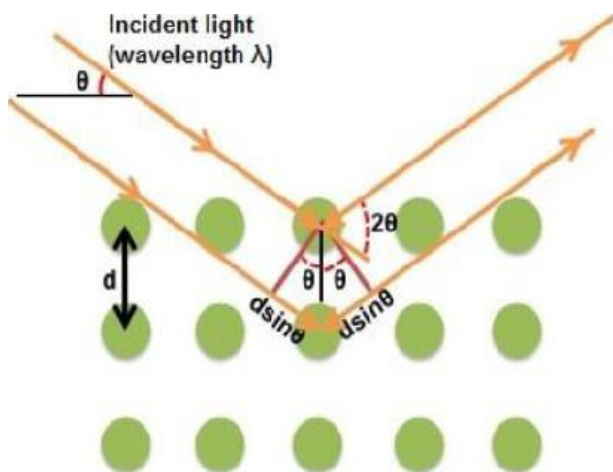Braggangle and **d** is the interplanar spacing.

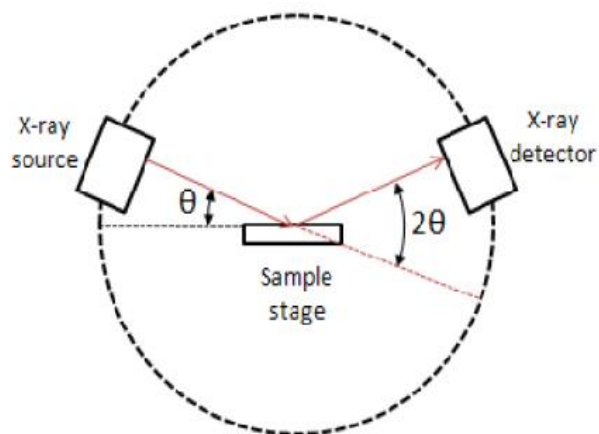| Fig 3.2: Illustration of Bragg's law | Fig 3.3: Schematic of X-ray Diffractometer. |

• **Applications:**

a)   Measurement of interplanar spacing between two atomic planes.

b)   Determination of orientation of single crystal.

c)   Determination of crystal structure for an unknown material.

d)   Measurement of particle size, phase and internal stress etc.

A Rigaku Ultima III X-ray diffractometer was used for recording the diffraction pattern of the samples in θ-2θ configuration with Cu Kα radiation (λ =1.5404 Å) operated at 40 KV voltage and 30 mA current. A photographic image of X-ray diffractometer is shown in Fig 3.4.

Fig 3.4: Experimental set up of X-Ray Diffractometer.

3.3 Analysis of absorbance spectra and molecular vibrations:

3.3.1 Fourier transform infrared spectroscopy (FTIR):

FTIR Spectroscopy, fourier-transform infrared spectroscopy, is concerned with the vibration of molecules. Each functional group has its own discrete vibrational energy which can be used to identify a molecule through the combination of all of the functional groups. This makes FTIR microscopy ideal for sample ID, multilayer film characterization, and particle analysis.

The electromagnetic spectrum consists of different regions corresponding to different energy (E), frequency (v), and wavelength (λ) ranges as seen in Figure 1. The unit for near-, mid-, and far-infrared, the wavenumber (cm^{-1}), is derived from the inverse relationship between wavelength and frequency.
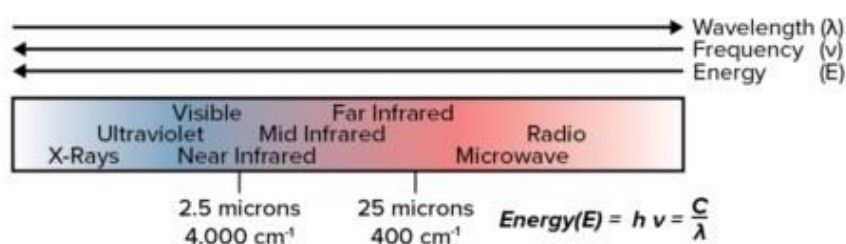

Fig. 3.12- Electromagnetic spectrum showing near and far infrared regions.

FTIR spectroscopy takes advantage of how IR light changes the dipole moments in molecules that correspond to a specific vibrational energy. Vibrational energy corresponds to two variables: reduced mass (μ) and bond spring constant (k). For k constant, we can look at C-C, C=C, and C≡C showing an increase of 800 cm^{-1} across the series. Substituting atoms in a C-C bond with nitrogen and oxygen causes a shift of 100 cm^{-1}. By looking at the two series, it can be seen that bond strength alters the wavenumbers more than mass.

Since every functional group is composed of different atoms and bond strengths, vibrations are unique to functional groups, and classes of functional groups (e.g. O-H and C-H stretches appear around 3200 cm^{-1} and 2900 cm^{-1}, respectively). A correlation chart with various

functional group vibrations can be seen. Since the collection of vibrational energy bands for all of the functional groups a molecule is unique to every molecule, these peaks can be used for identification using library searches of comprehensive sample databases.

Working principle and different parts of FTIR

The three major parts of an FTIR are the source, interferometer, and detector The source is typically a broadband emitter such as a mid-IR ceramic source (50-7,800 cm-1), a near-IR halogen lamp (2,200 – 25,000 cm-1), or a far-IR mercury lamp (10-700 cm-1). The interferometer is the heart of FTIR and consists of a beam-splitter, a stationary mirror, a moving mirror, and a timing laser (box in figure 4). The beam-splitter splits the light from a source into two paths with half the light going to a stationary mirror and the other half going to a moving mirror. In many FTIR systems, the beam-splitter is placed at 45 degrees to the incident beam, but for high throughput applications, a low angle interferometer is preferred as the P and S polarizations converge close to the Brewster's Angle. Common beam-splitter materials are KBr (375 – 12,000 cm-1) for mid-IR, Quartz (4,000 – 25,000 cm-1) for near-IR, and Mylar (30 – 680 cm-1) for far-IR. The beams from the moving and stationary mirrors are recombined back at the beam-splitter and steered toward the sample. The difference in the path of the mirrors causes constructive and destructive interference over the course of time it takes for the moving mirror to make a pass. The signal versus mirror position (and, thus, time) is called an interferogram. A laser is used to determine the position of the moving mirror using the precisely known wavelength of the laser (Figure 5). He-Ne lasers are the industry norm due to their excellent wavelength stability compared to solid-state or diode lasers. This laser stability allows for spectral additions, library searches, and other functions that need high wavenumber accuracy.
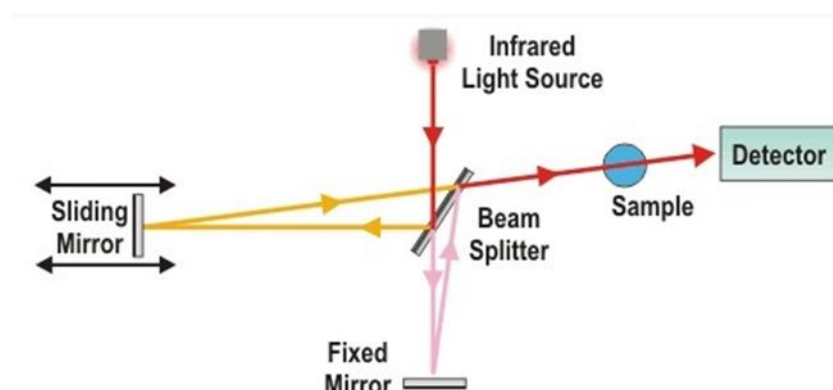
Fig. 3.13- Different parts and working of FTIR spectroscopy

- **Near infrared**

The Near-IR portion of the electromagnetic spectrum falls between 4,000 to 12,800 cm. This region consists of overtones (two of the same vibrational modes occurring simultaneously) and combinations (two different vibrational modes occurring simultaneously). Since these modes are not strictly quantum mechanically allowed, the intensity of the modes is often quite low. These spectra are often complex, and chemometric techniques, such as multivariate analysis, are used. In spite of the drawbacks, there are clear advantages to Near-IR spectroscopy. Firstly, the path length of the light is such that bulk samples can be analyzed with little to no sample preparation. Secondly, water does not affect signal as it does in mid-IR.

- **Far infrared**

The Far Infrared region lies between 10 cm^{-1} and 700 cm^{-1}. The bonds that show in this region are 3+ atom functional groups, such as -C-C-C- bending, and lattice vibrations in crystalline materials. Since these are highly dependent on conformation or crystal structure, materials with the same chemical structure, but different crystal structures may be distinguished using Far-IR.

3.3 Morphological analysis:

3.3.1 Field Emission Scanning Electron Microscope (FESEM):

The word microscope is derived from the Greek micros(small) and scope (look at). From the discovery of science there has been an interest in being able to look at smaller and smaller details of the world around us. Our human eye provides the extreme limitation in microscopy. It has a resolution ρeye of ~0.1 mm, which is equivalent to the diameter of a human hair. This means that two small objects placed about 20 cm from the eye can be viewed as distinct when they are ~0.1 mm apart. The limitation arises from the intrinsic magnification power of human eye and the separation of the sensing elements on the retina. An optical microscope has a resolution ρopt and improvement of ρopt than that of the unaided eye can be done in a way which is limited by the wavelength of the light used to illuminate the object. For visible light, this corresponds to ρopt ~0.2 μm. That's why below 0.2 μm, we cannot visualize objects through optical microscope. A FESEM is an electron microscope which uses electron beam liberated by field emission source instead of light.

Electrons will not travel far through air and electron microscopes are usually vacuum based instruments. Image formation in the SEM depends on the signals produced from the electron beam and specimen interactions. These interactions can be classified into two major categories: elastic interactions and inelastic interactions. Elastic scattering results from the deflection of the incident electron by the atomic nucleus or outer shell electrons of the specimen. This kind of interaction is characterized by very small amount of energy loss during the collision and by a wide-angle directional change of the scattered electron. Incident electrons that are elastically scattered through an angle of more than 90° are called backscattered electrons (BSE), and produce a useful signal for imaging the sample. Inelastic scattering occurs through a variety of interactions between the incident electrons and the electrons and atoms of the sample and results in the primary beam electron transferringconsiderable amount of energy to that atom. The amount of energy loss depends on whetherthe specimen electrons are excited singly or collectively and on the

binding energy of theelectron to the atom. The most widely used signal produced by the interaction of the primaryelectron beam with the specimen is the *secondary electron emission* signal. When the primarybeam strikes the sample surface causing the ionization of specimen atoms, loosely boundelectrons may be emitted and these are referred to as secondary electrons. As they have lowenergy, typically an average of around 3–5 eV, they can only escape from a region within afew nanometers of the material surface. These can be used to give information about thesurface topography, morphology of the sample with good resolution. In addition to thesesignals, several other signals are produced when an electron beam strikes a sample,including the emission of *continuous x-rays, characteristic x-rays, Auger electrons and cathodoluminescence.*
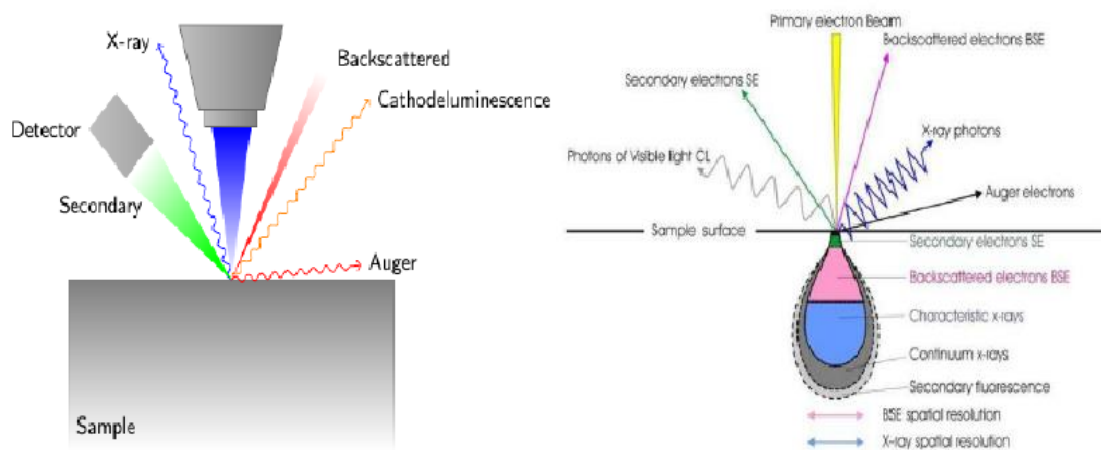
Fig 3.11: Interaction of electron beam with matter.

- **Configuration of FESEM:**

Fig 3.11 shows the total components of Field emission scanning electron microscope in details. It consists of electron gun to generate electron beam, electromagnetic lenses, and aperture to focus the electron beam, detector, and vacuum system.

- **Electron Gun***:*

The electron gun produces a stable electron beam with high current, small spot size, adjustable energy and small energy dispersion. The first-generation SEM systems generally used thermionic emission sources like tungsten "hairpin" ($\Phi=4.5eV$) or lanthanum hexaboride (LaB_6) ($\Phi=2.4eV$) cathodes, but for the modern SEMs, the trend

is to use field emission sources, which provide enhanced current and lower energy dispersion. Emitter lifetime is another important issue for selection of electron sources. The most widely used electron gun is composed of three parts: a V-shaped hairpin tungsten filament (the cathode), a Wehnelt cylinder and an anode, as shown in figure 3.13. Thermionic sources require a high temperature to overcome the work function of the metal sothat the electrons can escape from the cathode. Though they are inexpensive and the requirement of vacuum is relatively low but there are certain disadvantages, such as short lifetime, low brightness, and large energy spread which restrict their applications. For modern electron microscopes, field emission electron guns (FEG) are a good alternative for thermionic electron guns. In the FEG, a single crystal tungsten wire with very sharp tip is used as the electron source. In this system, a strong electric field forms on the finely oriented tip and the electrons are drawn toward the anodes forms concentrated electron beam.

- **Electron Lenses:**

Electron beam can be focused by electrostatic or magnetic field. But electron beam controlledby magnetic field has smaller aberration, so only magnetic field is employed in SEM system. Coils of wire, known as "electromagnets" are used to produce magnetic field and the trajectories of the electrons can be adjusted by the current applied on these coils.

- **Condenser lens:**

The electron beam will diverge after passing through the anode plate from the emission source. By using the condenser lens, the electron beam is converged and collimated into a relatively parallel stream. A magnetic lens generally consists of two rotationally symmetric iron pole pieces in which there is a copper winding which provides magnetic field. There is a hole in the center of pole pieces that allows the electron beam to pass through. A lens-gap separates the two pole pieces, at which the magnetic field focuses the electron beam. The position of the focal point can be controlled by adjusting the condenser lens current.
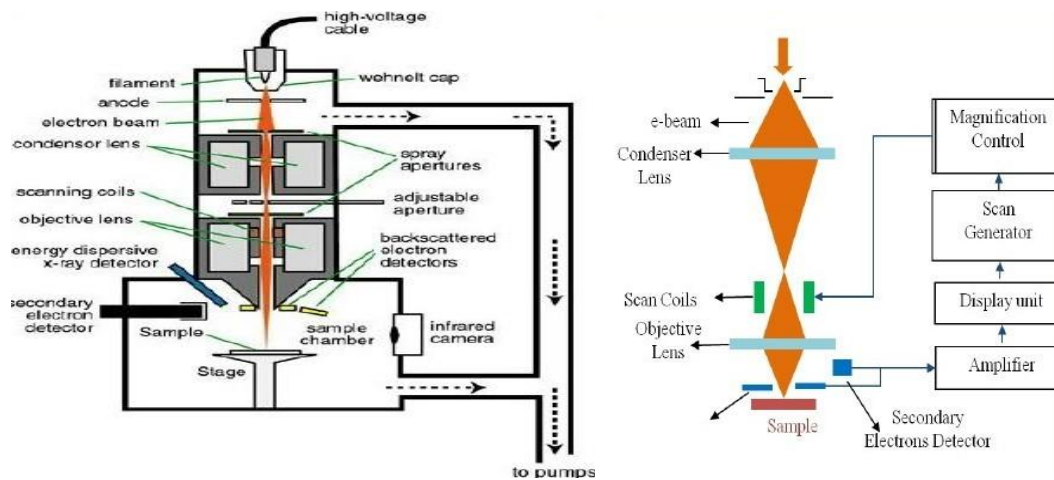
Fig 3.12: Configuration of FESEM and its different components

- **Scan Coils:**

The scan coils deflect the electron beam over the object according to a zigzag pattern. The formation of the image on the monitor occurs in synchrony with this scan movement. The scan velocity determines the refreshing rate on the screen and the amount of noise in the image. Scan coils often consist of upper and lower coils, which prevent the formation of a circular shadow at low magnification.

- **Objective lens:**

The objective or "probe forming" lens is located at the base of electron column just above sample. The beam is again divergent after passing through the apertures below the condenser lens and must be convergent again. The objective lens focuses the electron beam onto the sample and controls final size and position.

- **Sample preparation:**

As we mentioned earlier that FESEM is vacuum based instrument, so sample must be vacuum tolerant. In addition to that, strong radiation by electrons can damage or destroy a sample through heating or other effects. Even in quite good vacuum (10^{-8} mbar), samples can become coated with gold/platinum in the microscope to retain the true surface details. Some samples, those are insulating in nature, are charged up under the electron beam and repel the incoming electron beam. This degrades the resolution and usually requires some prevention technique such as coating the sample with a conducting layer.

Fig 3.13: FESEM (Hitachi S-4800) set up.

3.4. Crystalline phase Analysis:

3.4.1. Fourier Transform Infrared Spectroscope (FTIR):

FT-IR stands for Fourier Transform InfraRed, the preferred method of infrared spectroscopy. In infrared spectroscopy, IR radiation is passed through a sample. Some of the infrared radiation is absorbed by the sample and some of it is passed through (transmitted). The resulting spectrum represents the molecular absorption and transmission, creating a molecular fingerprint of the sample. Like a fingerprint no two unique molecular structures produce the same infrared spectrum. This makes infrared spectroscopy useful for several types of analysis.

So, what information can FT-IR provide?

• It can identify unknown materials

• It can determine the quality or consistency of a sample

• It can determine the amount of components in a mixture

This booklet is an introduction to the concepts behind FT-IR spectroscopy. It covers both the basic theory of FT-IR and how it works as well as discussing some the practical aspects of FT-IR use.
We hope that it gives you a good understanding of the importance and usefulness of this powerful technique.

3.4.2. Why Infrared Spectroscopy?

Infrared spectroscopy has been a workhorse technique for materials analysis in the laboratory for over seventy years. An infrared spectrum represents a fingerprint of a sample with absorption peaks which correspond to the frequencies of vibrations between the bonds of the atoms making up the material.

Because each different material is a unique combination of atoms, no two compounds produce the exact same infrared spectrum. Therefore, infrared spectroscopy can result in a positive identification (qualitative analysis) of every different kind of material. In addition, the size of the peaks in the spectrum is a direct indication of the amount of material present. With modern software algorithms, infrared is an excellent tool for quantitative analysis.

Fourier Transform Infrared (FT-IR) spectrometry was developed in order to overcome the limitations encountered with dispersive instruments. The main difficulty was the slow scanning process. A method for measuring all of the infrared frequencies simultaneously, rather than individually, was needed. A solution was developed which employed a very simple optical device called an interferometer.

The interferometer produces a unique type of signal which has all of the infrared frequencies "encoded" into it. The signal can be measured very quickly, usually on the order of one second or so. Thus, the time element per sample is reduced to a matter of a few seconds rather than several minutes.

Most interferometers employ a beam splitter which takes the incoming infrared beam and

divides it into two optical beams. One beam reflects off of a flat mirror which is fixed in place. The other beam reflects off of a flat mirror which is on a mechanism which allows this mirror to move a very short distance (typically a few millimeters) away from the beam splitter. The two beams reflect off of their respective mirrors and are recombined when they meet

back at the beam splitter. Because the path that one beam travels is a fixed length and the other is constantly changing as its mirror moves, the signal which exits

the interferometer is the result of these two beams "interfering" with each other. The resulting signal is called an interferogram which has the unique property that every data point (a function of the moving mirror position) which makes up the signal has information about every infrared frequency which comes from the source.

This means that as the interferogram is measured, all frequencies are being measured simultaneously. Thus, the use of the interferometer results in extremely fast measurements. Because the analyst requires a frequency spectrum (a plot of the intensity at each individual frequency) in order to make an identification, the measured interferogram signal cannot be interpreted directly. A means of "decoding" the individual frequencies is required. This can be accomplished via a well-known mathematical technique called the Fourier transformation. This transformation is performed by the computer which then presents the user with the desired spectral information for analysis.

3.4.3. The Sample Analysis Process

The normal instrumental process is as follows:

* The Source: Infrared energy is emitted from a glowing black-body source. This beam passes through an aperture which controls the amount of energy presented to the sample (and, ultimately, to the detector).

** The Interferometer: The beam enters the interferometer where the "spectral encoding" takes place. The resulting interferogram signal then exits the interferometer.

*** The Sample: The beam enters the sample compartment where it is transmitted through or reflected

off of the surface of the sample, depending on the type of analysis being accomplished. This is where specific frequencies of energy, which are uniquely characteristic of the sample, are absorbed.

**** The Detector: The beam finally passes to the detector for final measurement. The detectors used are specially designed to measure the special interferogram signal.

***** The computer: The measured signal is digitized and sent to the computer where the Fourier transformation takes place. The final infrared spectrum is then presented to the user for interpretation and any further manipulation.

Because there needs to be a relative scale for the absorption intensity, a background spectrum must also be measured. This is normally a measurement with no sample in the beam. This can be compared to the measurement with the sample in the beam to determine the "percent transmittance."

This technique results in a spectrum which has all of the instrumental characteristics removed. Thus, all spectral features which are present are strictly due to the sample. A single background measurement can be used for many sample measurements because this spectrum is characteristic of the instrument itself.
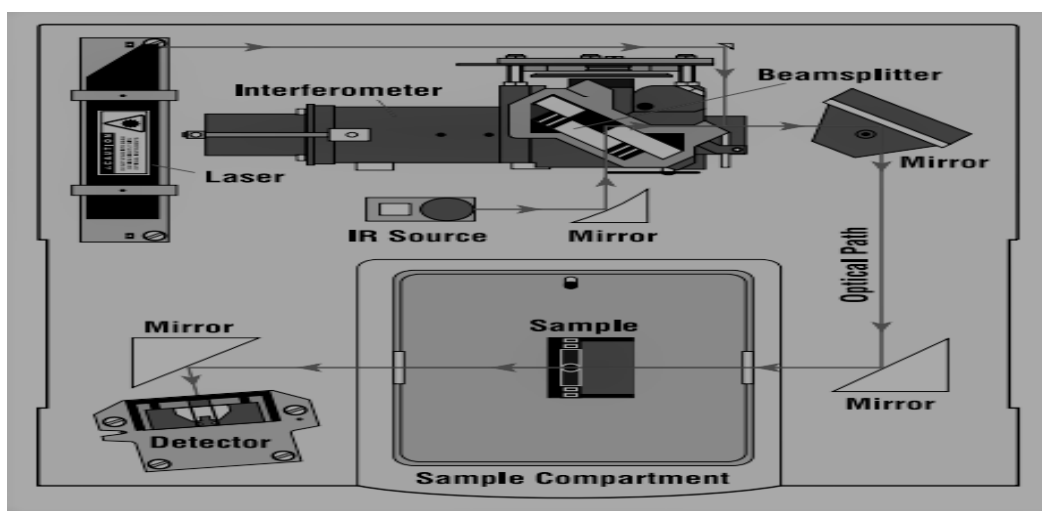
Fig 3.4.3 A Simple Spectrometer Layout

3.5.1. Measurements inCathode Ray Oscilloscope (CRO)

The cathode ray oscilloscope (CRO) is a type of electrical instrument used for measuring and analysing waveforms and other electronic and electrical phenomena. It is a quick X-Y plotter that displays the input signal vs another signal or versus time. CROs are used to analyse waveforms, transients, phenomena, and other time-varying values ranging from extremely low to radio frequencies.

The CRO is mostly powered by voltages. Thus, additional physical quantities such as current, strain, acceleration, and pressure are transformed into voltage via a transducer and shown on a CRO. It is also used to determine waveforms, transient phenomena, and other time-varying quantities ranging from extremely low frequencies to radio frequencies.

The CRO includes a Stylus (a bright spot) that moves across the display surface in response to an input voltage. A stream of electrons striking a fluorescent screen produces this brilliant spot. The CRO's standard configuration employs a horizontal input voltage that is an internally produced ramp voltage known as "time base."

The horizontal voltage moves the bright spot across the display area or screen in a horizontal manner from left to right on a regular basis. The voltage under consideration is the vertical voltage. The vertical voltage pushes the glowing spot on the screen up and down. When the input voltage moves very quickly on the screen, the display seems motionless. Thus, CRO allows for the visualization of time-varying voltage.

Construction of Cathode Ray Oscilloscope

The main parts of the cathode ray oscilloscope are as follows.

    Cathode Ray Tube
    Electronic Gun Assembly
    Deflecting Plate
    Fluorescent Screen For CRT
    Glass Envelop
Their parts are explained below in details.

. Cathode Ray Tube

The cathode ray tube is the vacuum tube which converts the electrical signal into the visual signal. The cathode ray tube mainly consists the electron gun and the electrostatic deflection plates (vertical and horizontal). The electron gun produces a focused beam of the electron which is accelerated to high frequency.

The vertical deflection plate moves the beams up and down and the horizontal beam moved the electrons beams left to right. These movements are independent to each other and hence the beam may be positioned anywhere on the screen.

. Electronic Gun Assembly

The electron cannon emits electrons in the shape of a beam. The heater, cathode, grid, pre-accelerating anode, focusing anode, and accelerating anode are the key components of an electron cannon. Layers of barium and strontium are formed on the cathode's end to achieve strong electron emission at low temperatures.

An electron is emitted from the cathode grid and then travels through the control grid. Typically, the control grid is a nickel cylinder with a centre axis that is co-axial with the CRT axis. It regulates the intensity of the electron emitted by the cathode.

A strong positive voltage given to the pre-accelerating or accelerating nodes accelerates the electron as it passes through the control grid.
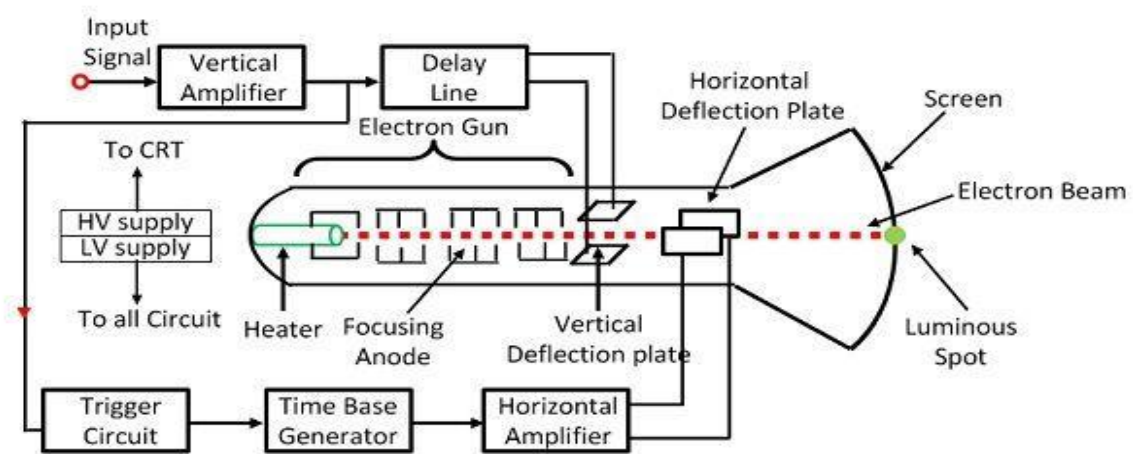
The electron beam is focused on focusing electrodes and then passes through the vertical and horizontal deflection plates and then goes on to the fluorescent lamp. The pre-accelerating and accelerating anode are connected to 1500v, and the focusing electrode is connected to 500 v. There are two methods of focusing on the electron beam. These methods are

- Electrostatic focusing
- Electromagnetic focusing.

Working of Cathode Ray Oscilloscope

The electron cannon injects one electron, which travels through the control grid. The intensity of electrons in the vacuum tube is controlled by the control grid. When the control grid has a high negative potential, just a few electrons can travel through it. As a result, a faint area appears on the lightning screen. The bright spot is formed when the negative potential on the control grid is low. As a result, the intensity of light is determined by the negative potential of the control grid.

The electron beam passes through the focusing and accelerating anodes once the control grid is moved. Because the accelerating anodes have a high positive potential, the beam is converged at a location on the screen.

After leaving the accelerating anode, the beam is affected by the deflecting plates. The beam forms a spot in the centre when the deflecting plate is at zero potential. When a voltage is provided to the vertical deflecting plate, the electron beam concentrates vertically, and when a voltage is applied horizontally, the light spot is deflected horizontally.
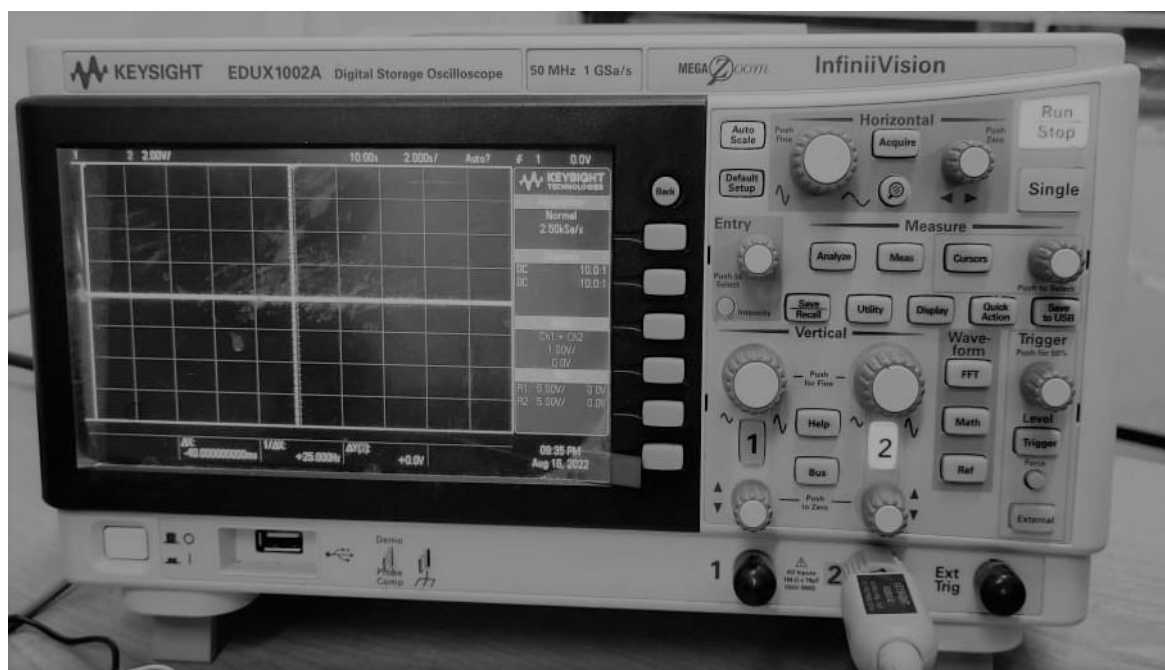
Fig 3.5.2 Digital Cathode Ray Oscilloscope (CRO)

Chapter -4

Lead-Free Double

Perovskite Cs2AgBiBr6

application for energy

harvesting application

Abstract

In order to meet the ever-increasing call for alternative energy, a plethora of novel materials have been explored to harvest energies. Amongst them, organic–inorganic halide perovskites belong to a relatively new class of compounds. In this work, we have prepared Cs2AgBiBr6 cubes via solution process and explored its candidature in energy harvesting. Piezoelectric nanogenerator (PNG) based on the composite of Cs2AgBiBr6 and poly (vinylidene fluoride) (PVDF) showed noticeable output performance. To get benchmark level output response, concertation of perovskite was optimized in composites. PNG fabricated with 3.0 wt% Cs2AgBiBr6 in PVDF exhibited an instantaneous output voltage of ~200 V and current of ~650nA. It also showed long cycle stability (10,000 cycles) and durability under robust conditions. Energy generated from the PNG was further utilized to charge a capacitor and light up commercial LEDs. As obtained results are of great importance and open the feasibility of novel smart device using this kind of perovskites.

4.1. Introduction

Rapid-growing industrialization and population all over the world in the past decades have fueled the total energy consumption. Most of the modern-day devices depend on conventional energy resources. Such dependency causes serious scarcity of resources, global warming, and severe environment pollution. Energy harvesting from various renewable environment benign resources is an effective way to circumvent the above issues. In addition to orthodox largescale energy harvesting arrangements, solar, piezoelectric, and triboelectric devices have been often explored for energy at ambient. Among these alternatives, piezoelectric nanogenerator (PNG) is very propitious tool which converts mechanical energy into electrical energy. Recently, lead halide perovskite materials, have garnered widespread attention in optoelectronics, due to their

typical features like high photoelectric conversion efficiency, large absorption coefficient, tunable band gap etc. However, researches on their piezoelectric features and their utility in modern devices are at initial stage. Spontaneous polarization in these halide perovskites can be attributed to their permanent dipoles provided by molecular cations. Kim et al. recently devised PNG using PVDF which delivered output of 2.7 V and 140 nA cm^{-2}. Realization of perovskite-based PNGs is very alluring because of their facile fabrication, mechanical robustness, and cost effectiveness. However, poor flexibility issues associated with perovskites limits their widespread utilization. Comprehension of flexible PNGs using perovskite as active material and polymers as flexible matrix is an effective pathway to dodge this issue. In this regard, usage of PVDF is well documented where PVDF presence not only provides the flexibility to device also boost up output power generation owing to its high piezoelectric constant. In this work, Cs2AgBiBr6 is synthesized by solution method. Amalgamating PVDF with as-synthesized Cs2AgBiBr6, PNGs are devised. Unlike to other reported works on this hybrid, no additional electrical poling process was performed here to achieve high output response. Concentration of perovskite in hybrid was controlled to obtain high output. Performance of these PNGs was monitored under several kind of applied stress and in different bending conditions. Performance of PNGs is elucidated on the basis of piezoelectric coefficient and electroactive phase constitution.

2. Experimental

2.1. Cs2AgBiBr6 synthesis

For the synthesis of Cs2AgBiBr6, we have modified our reported synthesis protocol. Initially a mixture was prepared by dissolving CsBr (0.259 mg) and PbBr2 (0.461 mg) within DMF (2 ml). Simultaneously, an oil phase was also prepared by adding hexane with oleic acid and n-octylamine. Thereafter, the oil phase was added slowly with the aforesaid mixture and stirred

for 5 min. Tert-butanol was further added immediately to initialize the demulsification. Finally, the precipitates were dried overnight in vacuum oven and collected.

2.1.2. PVDF-Cs2AgBiBr6 film preparation

1.5 gm PVDF pallets were added in acetone (12 ml) and DMF (8 ml) mixture. Afterwards, as synthesized Cs2AgBiBr6 with different concentration (3, 4, 5, 6 and 7 wt% (w/v)) was added to the above solution and stirred for 2 h at 70 °C. A yellow colored, homogeneous solution was prepared which was further solution drop casted on pre-cleaned glass slides. These coated substrates were kept in vacuum at 60 °C for overnight. Thereafter, films were peeled off from the glasses and used for device fabrication and various characterizations.

Depending on the concentration of Cs2AgBiBr6 in the composite film we have labelled the as prepared samples as PVDF (PVDF film only), PCS 3, PCS 4, PCS 5, PCS 6 and PCS 7 where attached numeric with PCs denotes weight percentage of Cs2AgBiBr6 in the composite.

2.1.3 Cs2AgBiBr6 FET characterization

The Cs2AgBiBr6 thin film FETs with different channel lengths were electrically characterized by using the computer interfaced Keithley 2602 under pulse mode measurement. The circuit connections along with the schematic of the FET are illustrated. The electrical contacts with the devices were made by using gold wirers and a portable probe station with spring-loaded contacts. All the electrical measurements were measured under ambient conditions. The transfer curves were measured by sweeping the gate voltage from -20 V to 40 V by keeping the Vds as constant at -40 V.
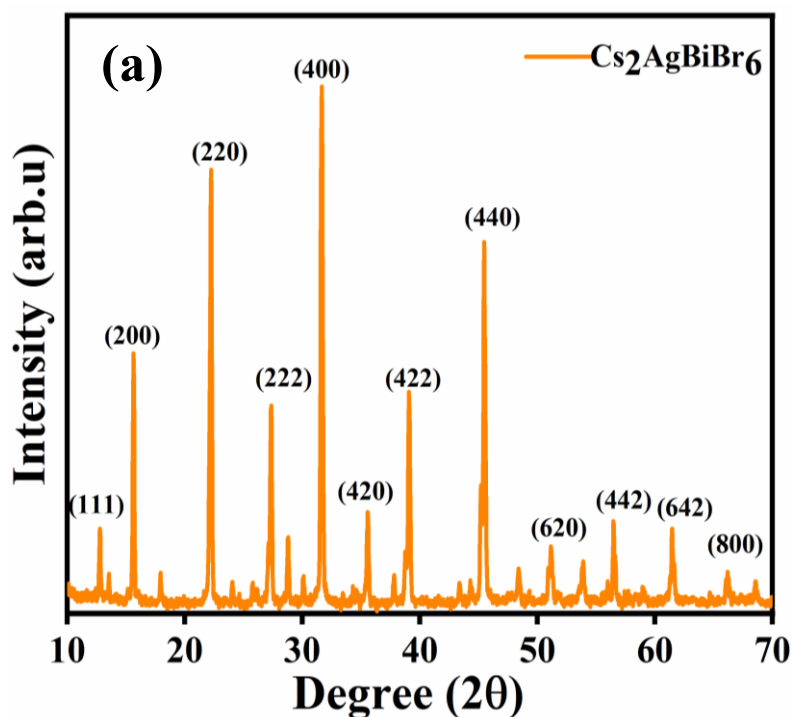
3. Results and discussion

Fig. 1. (a) XRD

XRD profile of the as synthesized Cs2AgBiBr6, presented in Fig. 1(a) shows diffraction peaks at 2θ ¼ 15.41°, 21.82°, 31.07°, 34.65° and 38.02° corresponds to (200), (220), (400), (420) and (442) planes respectively. Such positioning of the peaks agrees well with literature and confirms orthorhombic phase formation of Cs2AgBiBr6.
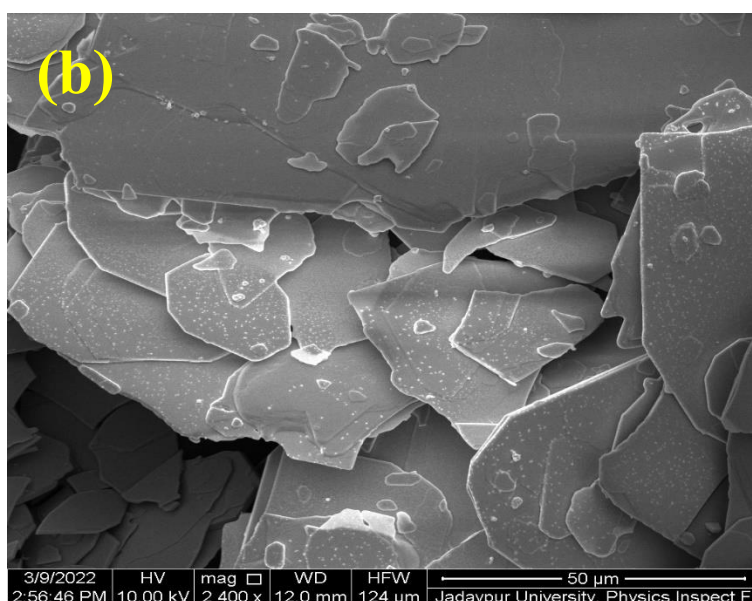

Fig. 1. (b) FESEM

FESEM image of Cs2AgBiBr6 shown in Fig. 1(b) depicts morphological uniformity of the synthesized products over large scale. One dimensional rod-like morphology with average diameter and length ~ 600 nm and 10–50 μm respectively is obvious from this image. Very small variance in average diameter the rods indicate homogeneous growth of Cs2AgBiBr6 crystal during synthesis
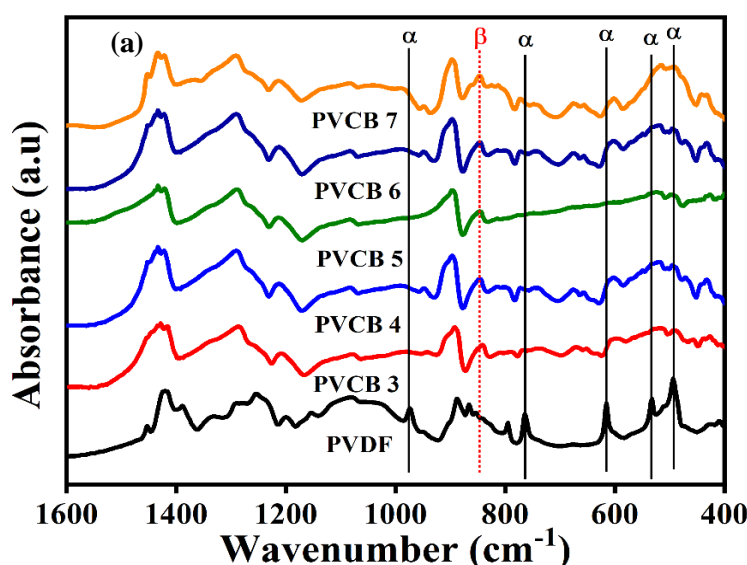

Fig .2 (a) FTIR spectra in the range 1600- 400

FTIR spectroscopy of the all the samples were carried out (Fig. 2a). Vibrational band at 796 cm− 1 is assigned to non-polar α phase of PVDF. Peak related to semi polar γ phase appeared at ~812 cm− 1. Vibrational band associated with desired electroactive β phase is observed at ~1279 and 841 cm− 1. Bare PVDF is largely composed of α and γ phase. β phase presence is very less in it. Intensity of the peaks related to α phase gradually decreases while intensity of electroactive phase increases with higher wt% (w/v) of perovskite incorporation. However, above 3 wt.% (w/v) perovskite loading, α phase started to reappear. Cs2AgBiBr6 acted as filler in PVDF. Interaction between positive surface charge of Cs2AgBiBr6 and –CH2-CF2– dipole in PVDF enhances electroactive phase percentage in the hybrid. Variation of Cs2AgBiBr6 loading in hybrids leads differences in such interaction and consequently in overall β phase constitution. β-phase constitution in samples is compared in Fig. (1a).
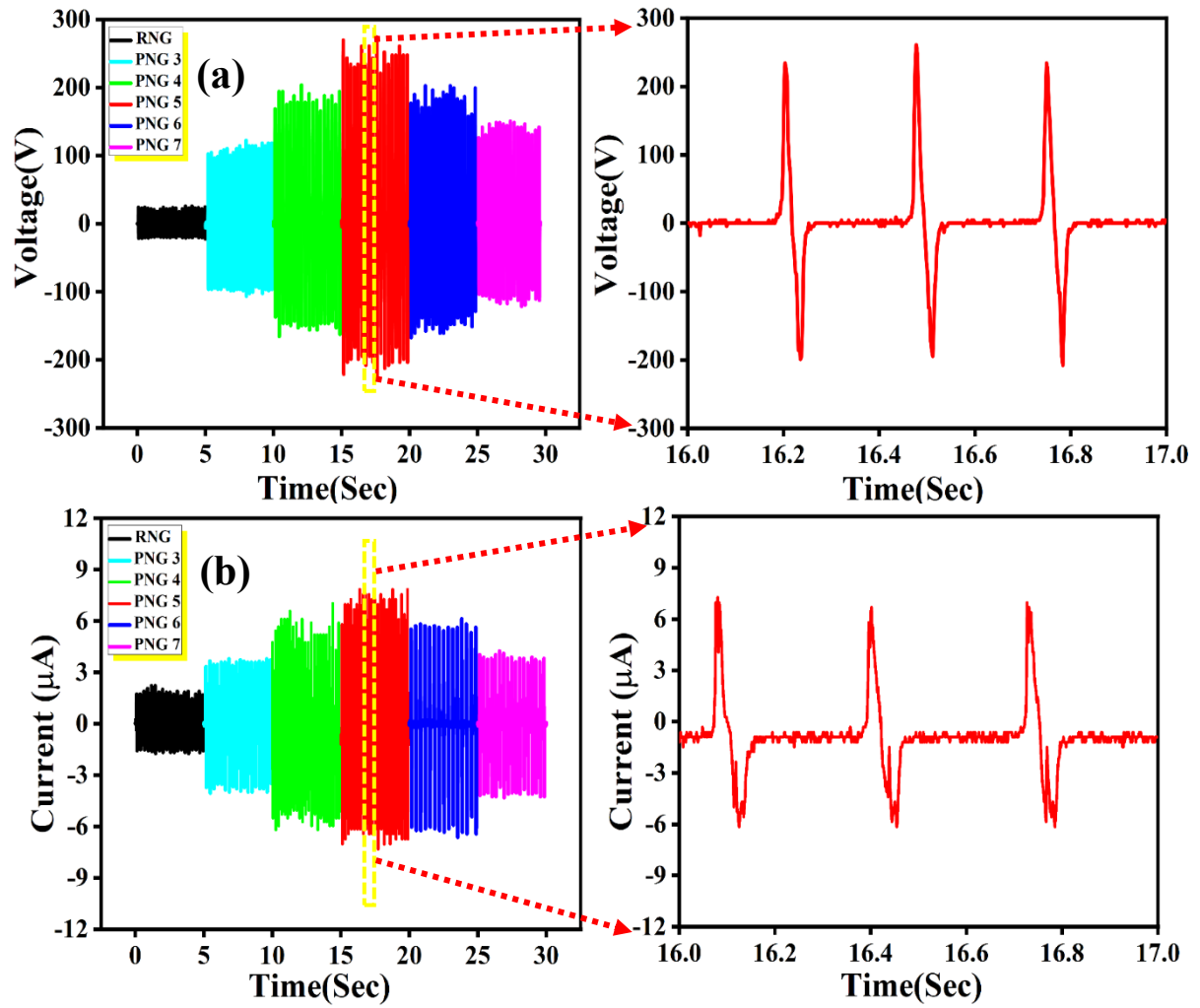
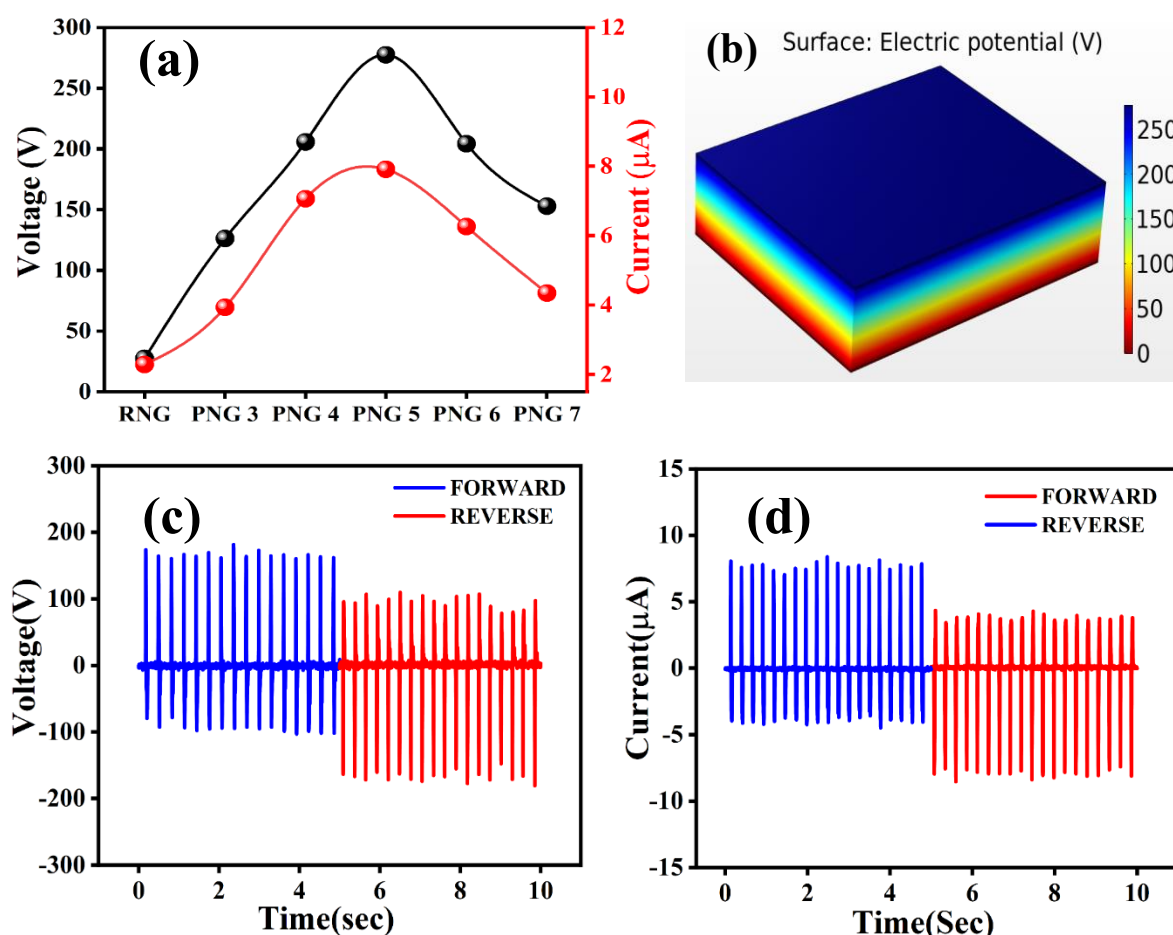Fig. 3. Instantaneous output (a) voltage and (b) current of PNGs.

FIG. 4 (a) voltage and current of PNGs.(b) Surface: Electrical Potential(V) (c) voltage in forward and reverse bias; (d) voltage in forward and reverse bias

To evaluate the piezoelectric performance, several PNGs were fabricated using PVDF-Cs2AgBiBr6 namely PNG 2, PNG 3, and PNG 4 where the end numeric with represents wt% (w/v) of Cs2AgBiBr6 in hybrid. Piezo response of PNGs under repeated mechanical forces are shown in Fig. 2a-b. No additional poling was performed here for performance enhancement. Instantaneous output voltages due to repeated hand hammering (pressure ~200 MPa) are gradually increased for PNGs up to 3 wt% Cs2AgBiBr6 loading in hybrid. Much higher loading of Cs2AgBiBr6 impacted adversely over output. PNG 3 delivered maximum

instantaneous output ~200 V. Instantaneous current profiles of PNGs mimic similar qualitative differences among themselves like voltage. With increasing Cs2AgBiBr6 content up to 3%, matrix β phases increased in PVDF matrix. To judge the figure of merit of PNG 3, its output response is compared with other reported works in Table. To check whether the registered output is truly piezo response or not, switching polarity test of PNG 3 also conducted. It delivered same level of output in reverse polarity (Fig. 3c). This result rules out the involvement of any kind of triboelectrification processes. Output performance was further studied as a function of load resistance (RL) at constant mechanical force (Fig. 3d). Instantaneous voltage drops across RL gradually increased with the increase of it and finally saturated at higher values. This saturated value at high resistance is equivalent to Voc. On the contrary, current follows the reverse trend. Short circuit current (Isc) decreased upon RL increment. RL vs. power graph is presented in Fig. (3d). PNG 3 delivered instantaneous power of ~10.5 μW at 3.5 MΩ.

Time to time recharge of our smart devices became our daily headache. Recharging these devices with the energy of PNG could be an easy alternative. Fig. 3 depicts the response of PNG 3 under several kind of human motion. For repeated finger tapping (pressure ~1 MPa), output ~5 V is registered (Fig. 3a). Zoom in view this (Fig. 3b) depicts sharp peak upon tapping. This peak reversed its direction on removal of tapping force. Bending of PNG 3 at an angle ~20˚generated ~8 V (Fig. 3c). Fig. 3d revels response over a cycle of press and release. Output response of PNG 3 at different bending condition is shown in Fig. S4 (see S.I.). Output of PNG 3 under human toe impression (pressure ~1.8 MPa) was also investigated (Fig. 3e). An instantaneous voltage ~4.7 V is registered. Upon removal of pressure, output shifted its direction (Fig. 3f). These results suggest the utility of PNG 3 in futuristic portable walking charger.
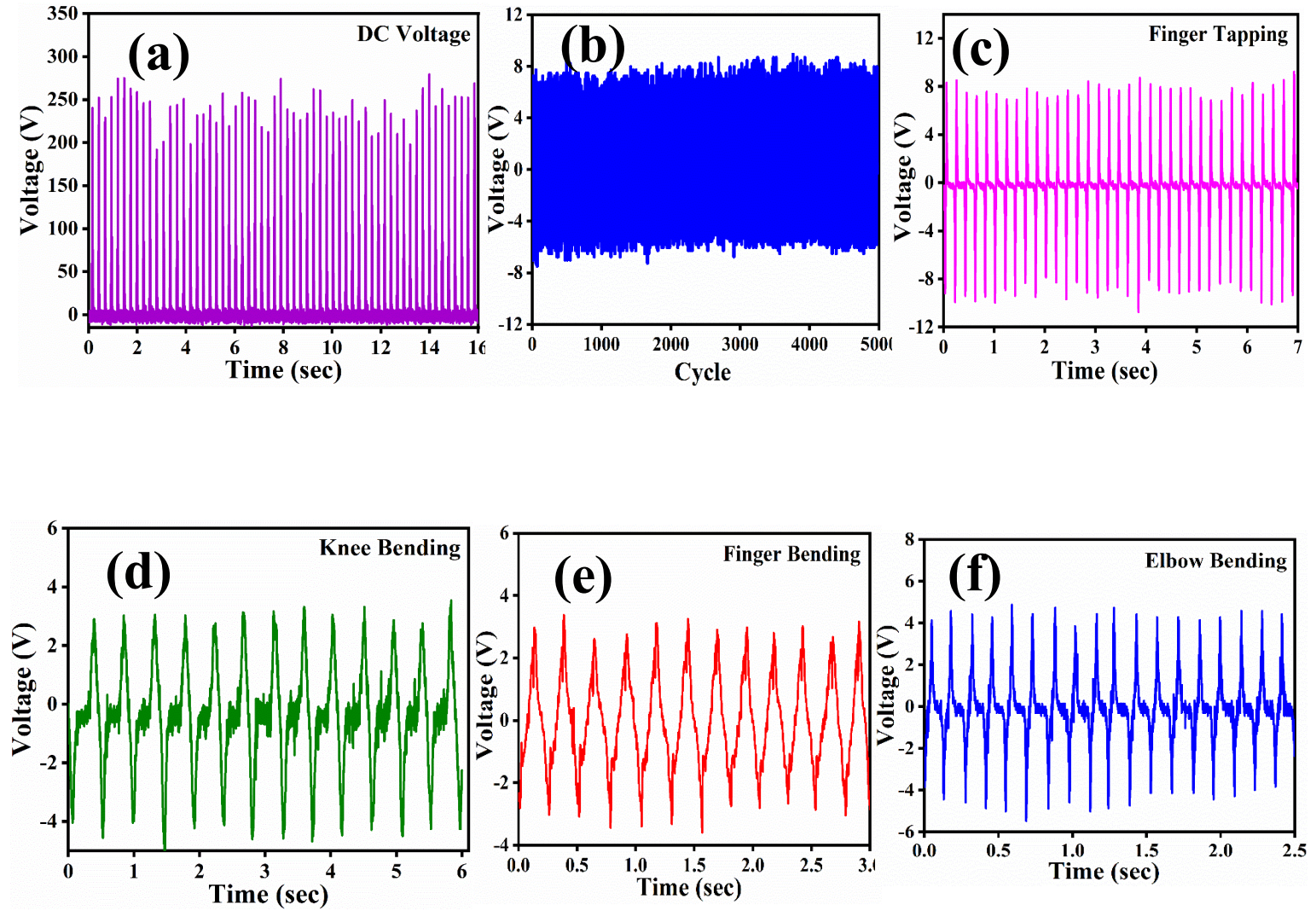
Fig. 4. Output voltage of PNG 5 (a) under the finger tapping (b) under toe pressing (c) due to air blower pressure (d) due to table fan air pressure (f) due to mobilevibration. (e) Digital image of the piezo-response under mobile vibration.

We regularly charge several rechargeable electronic gadgets from electricity. Replacing energy source for the devices with the energy of nanogenerator is a great alternate. We have fastened PNG 5 in one arm and contracted and expanded the arm regularly. Maximum output ~ 4 V is registered for contraction and expansion of arm (Fig. 4c). Upon contraction of arm, a pressure

is imparted on PNG 5 and it delivered ~4 V output voltage. With the release of pressure due to arm expansion, output voltage followed the reverse direction. Such result suggests the usage of PNG 5 as energy source in other human activity like foot striking, jogging etc. Going beyond pressing forces, ability of PNG 5 to detect bending force was also examined. Voltage vs. time graph presented in Fig. 7d for slight bending of PNG 5 by finger delivered output voltage of 8 V. Sharp peak was obtained under bending. Upon removal of bending, voltage peaks appeared in reversed direction (Please see supporting video SV3y). It is necessary to explore the suitability of PNG in real-life applications. To explore the suitability of the PNG 5 in real life applications, we have attached it upon a drum of a toy (Fig. 4e.). Output voltage was monitored in response to the repeated drum beats of the toy (Fig. 4f.). High output voltage ~5 V generation by PNG 5 under the gentle drum beats opens up its possibility to be used in real life applications. Several countries use wind energy to fulfil their internal energy demand. However, it involves huge wind mill, wind power and other associated machineries which limit their widespread usage. Performance of the PNG 5 was explored under gentle air form commercially available air blower. When an air blower of 800 Was held 15 cm above PNG 5, output voltage ~ 2 V is registered (Fig. 4c). This result suggests that PNG 5 can harvest energy from gentle air pressure and it can be used as in air pressure sensor. Fig. 8d reveals the output voltage ~ 0.8 V under table fan air pressure. It is interesting to note that voltage responses alter in opposite way due to the vibration caused by table fan air pressure. From the large assortment mechanical energy (energy from wind, acoustics, human movement, etc.) vibrational energy is of utmost valued energy due to its large accessibility at any instant. To check the ability of PNG 5 as vibration sensor, a mobile phone in vibration mode was kept on it. Output response of the device during mobile calling vibration included periodic alteration of positive and negative voltage peaks (~0.8 V) (Fig. 4e and f). When the vibration is in off mode, no response is registered. This result confirmed that PNG can detect mobile vibration and generate electrical

response. Besides piezoelectric analysis, high optical absorption of PCS 5 as compare to PVDF and perovskite ignites its usage as photodetector. Broad absorption in the visible region for PCS 5 is obvious from the figure which is attributed to the incorporation of Cs2AgBiBr6 in PVDF. Absorption in PVDF film solely is forbidden in this region. For the fabrication of photodetector, PCS 5 sample is drop casted over ITO coated PET substrate which serves as one electrode. Conducting carbon tape is pasted on the other side act as another electrode. Further, the entire system is encapsulated with PDMS which ensure flexibility of the device. Prior to all I–V measurement the device is kept under complete darkness which ensures equilibrium conditions attainment. I–V characteristics of photodetectors presented in Fig. 9a in both dark and light illumination condition were found to exhibit linear nature which signifies good ohmic character. These curves clearly suggest 2 folds increment in photocurrent under light as compared to the dark value. To use the device for self-powered light detector, piezoelectric energy harvesting under light was also examined. Response of the aforesaid device under periodic stress under light and dark condition showed discernible differences in the output characteristics. Output current vs time graph presented in Fig. 9b suggest an increment in average values of short circuit current under light illumination. Such kind of behavior from the device can be explained as follow: under visible light electron hole pair is generated in Cs2AgBiBr6. Photocurrent created from photogenerated extra carriers within the sample under light ensues an enhancement in short circuit current. Furthermore, the photogenerated electron moves within film and lead to local electromagnetic field enhancement. With such field improvement orientation of the dipoles in the film interrupts and reduction in open voltage is registered. For advance electronic application, a nanogenerator should not only show high output characteristics but also should exhibit long term stability and durability under robust conditions. Cyclic fatigue, an important issue related with nanogenerator was verified via by continuous periodical impacting of PNG 5 for several

months by the drum beats of a toy. No discernible diminishment is observed in the output characteristics even after 15,000

4. Conclusion

In nutshell, we have successfully fabricated piezoelectric nanogenerator using cube shaped $Cs_2AgBiBr_6$ nanoform and PVDF. Hybrid sample with 3 wt% perovskite in it showed maximum β-phase, nearly 2- fold of pristine PVDF. PNG based on this sample delivered instantaneous voltage ~200 V under repeated hand hammering on it. Performance of the same also examined under several basic human movements. Bending of PNG 3 by finger generated an output ~8 V. PNG 3 was also able to light up LEDs without external bias. These results highlight the potential applicability of this hybrid as foldable and wearable energy harvester and thereby its integration in smart devices.

References

[1] S.H. Lee, C.K. Jeong, G.T. Hwang, K.J. Lee, Nano Energy 14 (2015) 111–125.

[2] S. Li, J. Wang, W. Peng, L. Lin, Y. Zi, S. Wang, G. Zhang, Z.L. Wang, Adv. Energy Mater. 7 (2017) 1602832.

[3] A. Sultana, P. Sadhukhan, M.M. Alam, S. Das, T.R. Middya, D. Mandal, ACS Appl. Mater. Interfaces 10 (2018) 4121–4130.

[4] A. Gaur, S. Tiwari, C. Kumar, P. Maiti, Nanoscale Adv 1 (2019) 3200–3211.

[5] T. Paul, B.K. Chatterjee, S. Maiti, S. Sarkar, N. Besra, B.K. Das, K.J. Panigrahi, S. Thakur, U.K. Ghorai, K.K. Chattopadhyay, J. Mater. Chem. C. 6 (2018) 3322–3333.

[6] Y. Wang, M.I. Dar, L.K. Ono, T. Zhang, M. Kan, Y. Li, L. Zhang, X. Wang, Y. Yang, X. Gao, Y. Qi, Science 365 (2019) 591–595.

[7] A. Pan, Y. Li, Y. Wu, K. Yan, M.J. Jurow, Y. Liu, L. He, Mater. Chem. frontiers 3 (2019) 414–419.

[8] Y.C. Chen, H.L. Chou, J.C. Lin, Y.C. Lee, C.W. Pao, J.L. Chen, C.C. Chang, R.Y. Chi, T.R. Kuo, C.W. Lu, D.Y. Wang, J. Phys. Chem. C 123 (2019) 2353–2360.

[9] C.T. Huang, J. Song, W.F. Lee, Y. Ding, Z. Gao, Y. Hao, L.J. Chen, Z.L. Wang, J. Am. Chem. Soc. 132 (2010) 4766–4771.

[10] K.I. Park, M. Lee, Y. Liu, S. Moon, G.T. Hwang, G. Zhu, J.E. Kim, S.O. Kim, D. K. Kim, Z.L. Wang, K.J. Lee, Adv. Mater. 24 (2012) 2999–3004.

[11] L. Li, M. Zhang, M. Rong, W. Ruan, RSC Adv. 4 (2014) 3938–3943.

[12] X. Gao, M. Zheng, X. Yan, J. Fu, M. Zhu, Y. Hou, J. Mater. Chem. C 7 (2019) 961–967.

[13] S. Jana, S. Garain, S. Sen, D. Mandal, Phys. Chem. Chem. Phys. 17 (2015) 17429–17436.

[14] N.L. Meereboer, I. Terzic, K. Loos, Polym. Chem. 10 (2019) 1335–1343.

[15] A. Sultana, M.M. Alam, P. Sadhukhan, U.K. Ghorai, S. Das, T.R. Middya, D. Mandal,

Nano Energy 49 (2018) 380–392.

[16] R. Ding, H. Liu, X. Zhang, J. Xiao, R. Kishor, H. Sun, B. Zhu, G. Chen, F. Gao, X. Feng, J. Chen, Adv. Funct. Mater. 26 (2016) 7708–7716.

[17] T. Paul, B.K. Chatterjee, S. Maiti, N. Besra, S. Thakur, S. Sarkar, K. Chanda, A. Das, P.K. Sarkar, K. Sardar, K.K. Chattopadhyay, in: AIP Conference Proceedings, 1953, 2018, 030085-030089.

[18] T. Paul, B.K. Chatterjee, N. Besra, S. Thakur, S. Sarkar, K.K. Chattopadhyay, Mater. Today Proc. 5 (2018) 2234–2240.

[19] T. Paul, S. Maiti, N. Besra, B.K. Chatterjee, B.K. Das, S. Thakur, S. Sarkar, N.S. Das, K.K. Chattopadhyay, ACS Appl. Nano Mater. 2 (2019) 5942–5951.

[20] T. Yang, Y. Zheng, Z. Du, W. Liu, Z. Yang, F. Gao, L. Wang, K.C. Chou, X. Hou, W. Yang, ACS Nano 12 (2018) 1611–1617.

[21] B. Saravanakumar, S. Soyoon, S.-J. Kim, ACS Appl. Mater. Interfaces 6 (2014) 13716–13723.

[22] P. Martins, A.C. Lopes, S.L. Mendez, Prog. Polym. Sci. 39 (2014) 683–706.

[23] M.S. Sebastian, A. Larrea, R. Gonçalves, T. Alejo, J.L. Vilas, V. Sebastian, P. Martins, S. Lanceros-Mendez, RSC Adv. 6 (2016) 113007–113015.

[24] A. Peles, O. Aleksic, V.P. Pavlovi, V. Djokovic, R. Dojcilovic, Z. Nikolic, F. Marinkovic, M. Mitric, V. Blagojevic, B. Vlahovic, V.B. Pavlovic, Phys. Scripta 93 (2018) 105801.

[25] T. Paul, D. Das, B.K. Das, S. Sarkar, S. Maiti, K.K. Chattopadhyay, J. Hazard Mater. 380 (2019) 120855.

[26] X. Zhou, C. Shao, S. Yang, X. Li, X. Guo, X. Wang, X. Li, Y. Liu, ACS Sustain. Chem. Eng. 6 (2018) 2316–2323.

[27] P. Adhikary, S. Garain, D. Mandal, Phys. Chem. Chem. Phys. 17 (2015) 7275–7281.

[28] G. Kresse, J. Hafner, Phys. Rev. B 47 (1993) 558–561.

[29] G. Kresse, J. Hafner, Phys. Rev. B 49 (1994) 14251–14269.

[30] G. Kresse, J. Hafner, Comput. Mater. Sci. 6 (1996) 15–50.

[31] G. Kresse, J. Furthmüller, Phys. Rev. B 54 (1996) 11169–11186.

[32] P.E. Blochl, € Phys. Rev. B 50 (1994) 17953–17979.

[33] G. Kresse, D. Joubert, Phys. Rev. B 59 (1999) 1758–1775.

[34] J.P. Perdew, K. Burke, M. Ernzerhof, Phys. Rev. Lett. 77 (1996) 3865–3868.

[35] S. Grimme, J. Comput. Chem. 27 (2006) 1787–1799.

[36] S. Garain, T.K. Sinha, P. Adhikary, K. Henkel, S. Sen, S. Ram, C. Sinha,

D. Schmeißer, D. Mandal, ACS Appl. Mater. Interfaces 7 (2015) 1298–1307.

[37] A. Sultana, M.M. Alam, S. Garain, T.K. Sinha, T.R. Middya, D. Mandal, ACS Appl.

Mater. Interfaces 7 (2015) 19091–19097.

[38] P. Biswas, N.A. Hoque, P. Thakur, M.M. Saikh, S. Roy, F. Khatun, B. Bagchi, S. Das,

ACS Sustain. Chem. Eng. 7 (2019) 4801–4813.

[39] N.R. Alluri, A. Chandrasekhar, V. Vivekananthan, Y. Purusothaman, S. Selvarajan,

J.H. Jeong, S.J. Kim, ACS Sustain. Chem. Eng. 5 (2017) 4730–4738.

[40] S.K. Karan, R. Bera, S. Paria, A.K. Das, S. Maiti, A. Maitra, B.B. Khatua, Adv. Energy

Mater. 6 (2016) 1601016.

[41] J.H. Lee, H.J. Yoon, T.Y. Kim, M.K. Gupta, J.H. Lee, W. Seung, H. Ryu, S.W. Kim,

Adv. Funct. Mater. 25 (2015) 3203–3209.

[42] S. Ye, C. Cheng, X. Chen, X. Chen, J. Shao, J. Zhang, H. Hu, H. Tian, X. Li, L. Ma,

W. Jia, Nano Energy 60 (2019) 701–714.

[43] K.Y. Lee, D. Kim, J.H. Lee, T.Y. Kim, M.K. Gupta, S.W. Kim, Adv. Funct. Mater. 24

(2014) 37–43.

[44] K.I. Park, C.K. Jeong, J. Ryu, G.T. Hwang, K.J. Lee, Adv. Energy Mater. 3 (2013)

1539–1544.

[45] N.A. Hoque, P. Thakur, S. Roy, A. Kool, B. Bagchi, P. Biswas, M.M. Saikh,

F. Khatun, S. Das, P.P. Ray, ACS Appl. Mater. Interfaces 9 (2017) 23048–23059.

[46] V. Jella, S. Ippili, J.H. Eom, J. Choi, S.G. Yoon, Nano Energy 53 (2018) 46–56.

[47] X. Ren, H. Fan, Y. Zhao, Z. Liu, ACS Appl. Mater. Interfaces 8 (2016) 26190–26197.

[48] N.R. Alluri, B. Saravanakumar, S.J. Kim, ACS Appl. Mater. Interfaces 7 (2015)

9831–9840.

[49] S. Bairagi, S.W. Ali, Energy 198 (2020) 117385.

[50] C. Chen, Z. Bai, Y. Cao, M. Dong, K. Jiang, Y. Zhou, Y. Tao, S. Gu, J. Xu, X. Yin, W. Xu, Compos. Sci. Technol. 192 (2020) 108100.

[51] A. Biswas, S. Garain, K. Maity, K. Henkel, D. Schmeißer, D. Mandal, Polym. Compos. 40 (2019) E265–E274.

[52] S.H. Wankhade, S. Tiwari, A. Gaur, P. Maiti, Energy Rep. 6 (2020) 358–364.

[53] X. Zhou, K. Parida, O. Halevi, Y. Liu, J. Xiong, S. Magdassi, P.S. Lee, Nano Energy 72 (2020) 104676.

[54] Z. Yin, B. Tian, Q. Zhu, C. Duan, Polym 11 (2019) 2033.

[55] J. Martín, D. Zhao, T. Lenz, I. Katsouras, D.M. de Leeuw, N. Stingelin, Mater. Horiz. 4 (2017) 408–414.

[56] G. Melilli, D. Lairez, D. Gorsea, E. Garcia-Caurel, A. Peinado, O. Cavani, B. Boizot, M.-C. Clochard, Radiat. Phys. Chem. 142 (2018) 54–59.

[57] N. Jahan, Development of the Piezoelectric Properties of Poly(Vinylidene Fluoride) Based Ferroelectrics and Ferroelectrets Using Fillers and Mechanical Stretching, 2018.

[58] T.H. Kim, A.C. Arias, Characterization and Applications of Piezoelectric Polymers, 2015.

[59] H. Liu, J. Zhong, C. Lee, S.W. Lee, L. Lin, Appl. Phys. Rev. 5 (2018), 041306.

[60] T. Yamamoto, K. Urabe, H. Banno, Jpn. J. Appl. Phys. 32 (1993) 4272.

[61] R. Hinchet, S. Lee, G. Ardila, L. Montes, M. Mouis, Z.L. Wang, Adv. Funct. Mater. 24 (2014) 971–977.

[62] G.H. Kim, S.M. Hong, Y. Seo, Phys. Chem. Chem. Phys. 11 (2009) 10506–10512.

[63] J. Gomes, J.S. Nunes, V. Sencadas, S. Lanceros-Mendez, Smart Mater. Struct. 19 (2010), 065010.

[64] P. Martinsa, A.C. Lopes, S. Lanceros-Mendez, Prog. Polym. Sci. 39 (2014) 683–706.

Chapter 5

Conclusion and scope for future work

5.1 Conclusion

In conclusion, we have reported, for the first time, fabrication of piezoelectric nanogenerator using a new class of composited based on simple solution processed all inorganic perovskite Cs2AgBiBr6 and PVDF. Concentration of Cs2AgBiBr6 is varied in the composite to achieve benchmark level performance. Electroactive phase content, degree of crystallinity, piezoelectric coefficient, optical and energy harvesting features of the samples have been investigated thoroughly. Going beyond regular mechanical stretching and poling techniques, polar phase initiation in PVDF matrix is achieved by Cs2AgBiBr6 incorporation. Nucleation of the stable electroactive phase in PVDF changes with the subtle variation of Cs2AgBiBr6 in the composite and maximum β-phase is obtained for 5 wt% perovskite loading. High percentage of β-phase constitution ensures its candidature as an ideal material for piezoelectric energy-harvesting. Besides, electroactive phase induction, PVDF encapsulation improved the stability of perovskite rod and also ensured higher amount of light absorption. Several kinds of external stimulus were applied on the devices to check their piezoelectric response. Repeated hammering by hand over PNG 5 produced an output voltage of 120 V. Simple bending of the optimized device by finger generated an open circuit voltage 8 V. Potential of the device as a vibration sensor was also explored under mobile vibration, air blower and regular table fan. Optimized composite sample-based photodetector delivered much improved current under light than dark which suggest its promises in light detection. Coupling of the photoactive Cs2AgBiBr6 with PVDF ensures visible light detection and leads substantial change in piezoelectric output current by 3 times and voltage by 2 times. Such results promise the usage of hybrid material for multipurpose applications like piezoelectric energy harvesting, light detection and in hybrid devices and pave the way towards self-powered photodetector.

5.2 Scope for future work:

Nanotechnology refers any technology on a nanoscale that has applications in the real world. Nanotechnology encompasses the production and application of physical, chemical, and biological systems at scales staring from individual atoms or molecules to submicron dimensions, as well as the integration of the resulting nanostructures into larger systems. Nano technology is likely to have a profound impact on our economy and society in the early 21st century, comparable to that of semiconductor technology, information technology or, molecular biology. Science and technology research in nanotechnology promises breakthroughs in areas such as materials and manufacturing, nanoelectronics, medicine and healthcare, energy, biotechnology, information technology, and national security. It is widely felt that nanotechnology will be the next Industrial Revolution.

- This perovskite-halide composite is very promising in terms of their excellent optoelectronics and electrical property. These enable researchers to develop piezo-photoelectronic devices.

- We could make use of these materials to develop hybrid devices, which incorporate photo active sensor as well as piezo-nanogenerator.

- Large scale production of these perovskite materials has been a challenge since past. So, we need to find some easy route of synthesis. Here, we have used colloidal route of synthesis, which considered to be a promising alternative to other tedious processes.